

# Radial migration of the Sun in the Milky Way: a statistical study

C. A. Martínez-Barbosa,<sup>★</sup> A. G. A. Brown<sup>†</sup> and S. Portegies Zwart<sup>‡</sup>

*Leiden Observatory, Leiden University, PO Box 9513 Leiden, NL-2300 RA, the Netherlands*

Accepted 2014 October 7. Received 2014 September 30; in original form 2014 July 4

## ABSTRACT

The determination of the birth radius of the Sun is important to understand the evolution and consequent disruption of the Sun’s birth cluster in the Galaxy. Motivated by this fact, we study the motion of the Sun in the Milky Way during the last 4.6 Gyr in order to find its birth radius. We carried out orbit integrations backward in time using an analytical model of the Galaxy which includes the contribution of spiral arms and a central bar. We took into account the uncertainty in the parameters of the Milky Way potential as well as the uncertainty in the present-day position and velocity of the Sun. We find that in general, the Sun has not migrated from its birth place to its current position in the Galaxy ( $R_{\odot}$ ). However, significant radial migration of the Sun is possible (1) when the 2: 1 outer Lindblad resonance of the bar is separated from the corotation resonance of spiral arms by a distance  $\sim 1$  kpc, and (2) when these two resonances are at the same Galactocentric position and further than the solar radius. In both cases, the migration of the Sun is from outer regions of the Galactic disc to  $R_{\odot}$ , placing the Sun’s birth radius at around 11 kpc. We find that in general, it is unlikely that the Sun has migrated significantly from the inner regions of the Galactic disc to  $R_{\odot}$ .

**Key words:** Sun: general – Galaxy: kinematics and dynamics – open clusters and associations: general – solar neighbourhood.

## 1 INTRODUCTION

The study of the history of the Sun’s motion within the Milky Way gravitational field is of great interest to the understanding of the origins and evolution of the Solar system (Adams 2010) and the study of past climate change and extinction of species on the earth (Feng & Bailer-Jones 2013). The determination of the birth radius of the Sun is of particular interest in the context of radial migration and in the quest for the siblings of the Sun (Portegies Zwart 2009; Brown, Portegies Zwart & Bean 2010). The work in this paper is motivated by the possibility in the near future of combining large amounts of phase-space data collected by the *Gaia* mission (Lindgren et al. 2008) with data on the chemical compositions of stars (such as collected by the *Gaia*-ESO survey; Gilmore et al. 2012) in order to search for the remnants of the Sun’s birth cluster. Our approach is to guide the search for the Sun’s siblings by understanding in detail the process of cluster disruption in the Galactic potential, using state of the art simulations. One of the initial conditions of such simulations is the birth location, in practice the birth radius, of the Sun’s parent cluster. In this paper, we present a parameter study of the Sun’s past orbit in a set of fully analytical Galactic potentials and we determine the most likely birth radius of the Sun and by

how much the Sun might have migrated radially within the Milky Way over its lifetime.

The displacement of stars from their birth radii is a process called radial migration. This can be produced by different processes: interaction with transient spiral structure (Sellwood & Binney 2002; Minchev & Quillen 2006; Roškar et al. 2008), overlap of the dynamical resonances corresponding to the bar and spiral structure (Minchev & Famaey 2010; Minchev et al. 2011), interference between spiral density waves that produce short-lived density peaks (Comparetta & Quillen 2012), and interaction of the Milky Way disc with in-falling satellites (Quillen et al. 2009; Bird, Kazantzidis & Weinberg 2012).

Since radial migration is a natural process in the evolution of Galactic discs, it is very likely that the Sun has migrated from its formation place to its current position in the Galaxy. Wielen (1996) argued that the Sun was born at a Galactocentric distance of  $6.6 \pm 0.9$  kpc; roughly 2 kpc nearer to the Galactic Centre. He based his conclusions on the observation that the Sun is more metal rich by 0.2 dex with respect to most stars of the same age and Galactocentric position (Holmberg, Nordström & Andersen 2009) and the presence of a radial metallicity gradient in the Milky Way. Other studies also support the idea that the Sun has migrated from its birth place. Based on chemo-dynamical simulations of Galactic discs, Minchev, Chiappini & Martig (2013) found that the most likely region in which the Sun was born is between 4.4 and 7.7 kpc from the Galactic Centre.

However, if the metallicity of the Sun is not unusual with respect to the surrounding stars of the same age, it would no longer be valid

<sup>★</sup> E-mail: [cmartinez@strw.leidenuniv.nl](mailto:cmartinez@strw.leidenuniv.nl)

<sup>†</sup> E-mail: [brown@strw.leidenuniv.nl](mailto:brown@strw.leidenuniv.nl)

<sup>‡</sup> E-mail: [spz@strw.leidenuniv.nl](mailto:spz@strw.leidenuniv.nl)

to assume that the Sun migrated from the inner parts of our Galaxy. By improving the accuracy in the determination of the effective temperature of the stars in the data of the Geneva–Copenhagen Survey, Casagrande et al. (2011) found that those stars are on average 100 K hotter and, hence, 0.1 dex more metal rich. This result shifts the peak of the metallicity distribution function to around the solar value, thus casting doubt on the observation that the Sun is metal rich with respect to its surroundings. Further studies also support the idea that the Sun is not an unusual star (Gustafsson 1998, 2008; Gustafsson et al. 2010).

The idea that the Sun might not have migrated considerably has been explored by several authors. By solving the equations of motion of the Sun under the influence of a disc, a dark matter halo, spiral arms and the Galactic bar described by a multipolar term, Klačka, Nagy & Jurči (2012) found that the radial distance of the Sun varied between 7.6 and 8.1 kpc. They find migration only when the Sun corotates with the spiral arms and when these structures represent very strong perturbations. On the other hand, by using the method suggested by Wielen (1996), Mishurov (2006) found that the Sun might have been born at approximately 7.4 kpc from the Galactic Centre.

Has the Sun migrated considerably? And if so, what are the conditions that allow such radial migration? One way of solving these questions is by computing the motion of the Sun in the Galaxy backwards in time. Portegies Zwart (2009) used this technique to find that the Sun was born at a distance of  $r = 9.4$  kpc with respect to the Galactic Centre. He used an axisymmetric potential for modelling the Milky Way, which is not realistic and furthermore, he did not take into account the uncertainty in the current position and velocity of the Sun (with respect to the Galactic reference frame).

The aim of this paper is to address the question of the Sun’s birth radius by carrying out orbit integrations backward in time, using a more realistic model for the Galaxy which includes the contribution of spiral arms and a central bar. We account for the uncertainty in the parameters of the Milky Way potential as well as the uncertainty in the present-day position and velocity of the Sun. The resulting parameter study is used to obtain a statistical estimation of the Sun’s birth radius 4.6 Gyr ago. We use the *AMUSE* framework (Portegies Zwart et al. 2013) to perform our computations.

This paper is organized as follows: in Section 2, we describe the model that we use for the Milky Way. In Section 3, we provide a brief overview of the *AMUSE* framework and the modules we developed to compute potential past orbits of the Sun in the Galaxy. In Section 4, we present the methodology to survey possible past orbits of the Sun and thereby constrain its birth radius. In Section 5, we analyse the orbit integration results and address the question of whether or not the Sun has migrated in the Galaxy and the conditions that would allow a considerable radial migration. In Section 6, we discuss the results and in Section 7, we present our conclusions and final remarks.

## 2 GALACTIC MODEL

Since the past history of the structure of the Milky Way is unknown, we simply assume that the values of the Galactic parameters have been the same during the last 4.6 Gyr, i.e. during the lifetime of the Sun (Bonanno, Schlattl & Paternò 2002). We model the Milky Way as a fully analytical potential that contains an axisymmetric component together with a rotating central bar and spiral arms. We use the potentials and parameters of Allen & Santillán (1991) to model the axisymmetric part of the Galaxy, which consist of a central bulge, a disc and a dark matter halo. The values of the

**Table 1.** Parameters of the Milky Way model potential.

<i>Axisymmetric component</i>	
Mass of the bulge ( $M_b$ )	$1.41 \times 10^{10} M_\odot$
Scalelength bulge ( $b_1$ )	0.3873 kpc
disc mass ( $M_d$ )	$8.56 \times 10^{10} M_\odot$
Scalelength disc 1 ( $a_2$ )	5.31 kpc
Scalelength disc 2 ( $b_2$ )	0.25 kpc
Halo mass ( $M_h$ )	$1.07 \times 10^{11} M_\odot$
Scalelength halo ( $a_3$ )	12 kpc
<i>Central bar</i>	
Pattern speed ( $\Omega_{\text{bar}}$ )	40–70 km s <sup>-1</sup> kpc <sup>-1</sup>
Semimajor axis ( $a$ )	3.12 kpc
Axis ratio ( $b/a$ )	0.37
Mass ( $M_{\text{bar}}$ )	$9.8 \times 10^9$ – $1.4 \times 10^{10} M_\odot$
Orientation	20°
<i>Spiral arms</i>	
Pattern speed ( $\Omega_{\text{sp}}$ )	15–30 km s <sup>-1</sup> kpc <sup>-1</sup>
Locus beginning ( $R_{\text{sp}}$ )	3.12 kpc
Number of spiral arms ( $m$ )	2, 4
Spiral amplitude ( $A_{\text{sp}}$ )	650–1300 km <sup>2</sup> s <sup>-2</sup> kpc <sup>-1</sup>
Strength of the spiral arms ( $\epsilon$ )	0.02–0.06
Pitch angle ( $i$ )	12:8
Scalelength ( $R_\Sigma$ )	2.5 kpc
Orientation	20°

parameters of these Galactic components are shown in Table 1. For the central bar and spiral arms, we use the models presented in Romero-Gómez et al. (2011) and Antoja et al. (2011) as detailed below.

### 2.1 Central bar

The central bar of the Milky Way is modelled as a Ferrers bar (Ferrers 1877) which is described by a density distribution of the form

$$\rho_{\text{bar}} = \begin{cases} \rho_0 (1 - n^2)^k & n < 1 \\ 0 & n \geq 1 \end{cases}, \quad (1)$$

where  $n^2 = x^2/a^2 + y^2/b^2$  determines the shape of the bar potential, where  $a$  and  $b$  are the semimajor and semiminor axes of the bar, respectively. Here,  $x$  and  $y$  are the axes of a frame that corotates with the bar.  $\rho_0$  represents the central density of the bar and the parameter  $k$  measures the degree of concentration of the bar. Larger values of  $k$  correspond to a more concentrated bar. The extreme case of a constant density bar is obtained for  $k = 0$  (Athanasoula, Romero-Gómez & Masdemont 2009). Following Romero-Gómez et al. (2011), we use  $k = 1$ . For these models, the mass of the bar is given by

$$M_{\text{bar}} = \frac{2^{(2k+3)} \pi a b^2 \rho_0 \Gamma(k+1) \Gamma(k+2)}{\Gamma(2k+4)}, \quad (2)$$

where  $\Gamma$  is the Gamma function.

#### 2.1.1 Galactic bar parameters

**Number of bars** The inner part of the Galaxy has been extensively studied within the *COBE/DIRBE* (Weiland et al. 1994) and *Spitzer/GLIMPSE* (Churchwell et al. 2009) projects, which demonstrated that the centre of the Milky Way is a complex structure.

While the *COBE/DIRBE* data showed that the surface brightness distribution of the bulge resembles a flattened ellipse with a minor-to-major axis ratio of  $\sim 0.6$ , the *Spitzer/GLIMPSE* survey confirmed the existence of a second bar (Benjamin et al. 2005) which was previously observed by Hammersley et al. (2000). Since the longitude and length ratios of these bars are in strong disagreement with both simulations and observations, Romero-Gómez et al. (2011) suggested that there is only a single bar at the centre of the Milky Way, which was confirmed by the analysis of Martínez-Valpuesta & Gerhard (2011), who show that the observations of the central region of the Milky Way can be explained by one bar. Hence we take into account the contribution of only one bar in the potential model of the Milky Way, using the parameters as obtained from the *COBE/DIRBE* survey.

**Pattern speed** The value of the pattern speed of the bar is uncertain. From theoretical and observational data Dehnen (2000) concluded that  $\Omega_{\text{bar}} = 50 \pm 3 \text{ km s}^{-1} \text{ kpc}^{-1}$ ; however, Bissantz & Gerhard (2002) argued that a more suitable value for the pattern speed of the bar is  $60 \pm 5 \text{ km s}^{-1} \text{ kpc}^{-1}$ . Taking into account these values, we assume that the bar rotates as a rigid body with a pattern speed between 40 and 70  $\text{km s}^{-1} \text{ kpc}^{-1}$ .

**Semimajor axis and axis ratio** Based on the best-fitting model by Freudenreich (1998) and on the uncertainty in the current solar Galactocentric position,<sup>1</sup> the semimajor axis of the *COBE/DIRBE* bar is between 2.96 and 3.31 kpc. With these assumptions, the axis ratio of the bar is between 0.36 and 0.38. In our simulations, we maintain these two parameters constant with the values listed in Table 1.

**Mass and orientation of the bar** Several studies suggest that the mass of the *COBE/DIRBE* bar is in the range  $0.98\text{--}2 \times 10^{10} M_{\odot}$  (Matsumoto et al. 1982; Dwek et al. 1995; Zhao 1996; Weiner & Sellwood 1999). Given that the bar is formed from the bulge, we assume the mass of the bar is in the range  $9.8 \times 10^9\text{--}1.4 \times 10^{10} M_{\odot}$ .

The orientation of the bar is defined as the angle between its major axis and the line that joins the Galactic Centre with the current position of the Sun. We fixed this angle at  $20^{\circ}$  (Pichardo, Martos & Moreno 2004; Romero-Gómez et al. 2011; Pichardo et al. 2012), as illustrated in Fig. 1.

**Effect of a growing bar** From  $N$ -body simulations, it appears that bars in galaxies are formed during the first 1.4 Gyr of their evolution (Fux 2000; Polyachenko 2013). Thus, we assume that the bar was already present in the Milky Way when the Sun was formed 4.6 Gyr ago.

## 2.2 Spiral arms

The spiral arms in our Milky Way Models are represented as periodic perturbations of the axisymmetric potential. Following Contopoulos & Grosbøl (1986), the potential of such perturbations in the plane is given by

$$\phi_{\text{sp}} = -A_{\text{sp}} R e^{-R/R_{\Sigma}} \cos(m(\phi) - g(R)), \quad (3)$$

where  $A_{\text{sp}}$  is the amplitude of the spiral arms.  $R$  and  $\phi$  are the cylindrical coordinates of a star measured in a corotating frame with the spiral arms.  $R_{\Sigma}$  and  $m$  are the scalelength and the number

<sup>1</sup> We conservatively assume the uncertainty in the distance from the Sun to the Galactic Centre is 0.5 kpc.

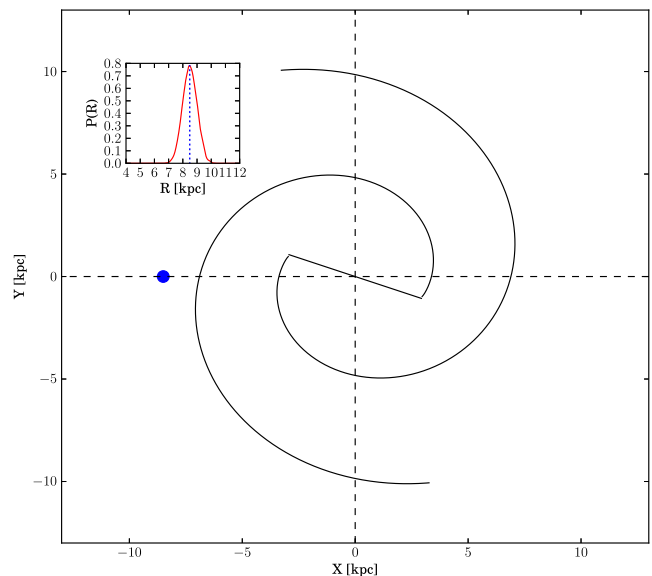


**Figure 1.** Configuration of the Galactic potential at the beginning of the backward integration in time. The spiral arms are assumed to start at the ends of the major axis of the bar. The blue circle is the current position of the Sun,  $r_{\odot} = (-8.5, 0)$  kpc. The angle the Sun–Galactic Centre line makes with respect to the semimajor axis of the bar is  $20^{\circ}$ . The inset shows the distribution of 5000 Galactocentric distances that were selected from a 3D Gaussian centred at the current phase-space coordinates of the Sun.

of spiral arms, respectively. The function  $g(R)$  defines the locus shape of the spiral arms. We use the same prescription as Antoja et al. (2011):

$$g(R) = \left( \frac{m}{N \tan i} \right) \ln \left( 1 + \left( \frac{R}{R_{\text{sp}}} \right)^N \right). \quad (4)$$

Here,  $N$  is a parameter which measures how sharply the change from a bar to a spiral structure occurs in the inner regions of the Milky Way.  $N \rightarrow \infty$  produces spiral arms that begin forming an angle of  $\sim 90^{\circ}$  with respect to the line that joins the two starting points of the locus (Antoja et al. 2011, as illustrated in Fig. 1 below). To approximate this case, we use  $N = 100$ .  $R_{\text{sp}}$  is the separation distance of the beginning of the spiral shape locus and  $\tan i$  is the tangent of the pitch angle.

### 2.2.1 Spiral arm parameters

**Pattern speed** Some studies point out that the spiral arms of the Milky Way approximately rotate with a pattern speed  $\Omega_{\text{sp}} = 25 \pm 1 \text{ km s}^{-1} \text{ kpc}^{-1}$  (e.g. Dias & Lépine 2005), while others argue that the value is  $\Omega_{\text{sp}} = 20 \text{ km s}^{-1} \text{ kpc}^{-1}$  (e.g. Martos et al. 2004). Since the pattern speed of the spiral arms is uncertain, we chose a range between 15 and 30  $\text{km s}^{-1} \text{ kpc}^{-1}$ , as in Antoja et al. (2011). In addition, we assume the spiral arms rotate as rigid bodies.

### Locus shape, starting point and orientation of the spiral arms

In the simulations, we adopt the spiral arm model obtained from a fit to the Scutum and Perseus arms. This is the so-called locus 2 in the work of Antoja et al. (2011). We also assume that the spiral structure starts at the edges of the bar. Hence  $R_{\text{sp}} = 3.12$  kpc. With this configuration, the angle between the line connecting the starting

point of the spiral arms and the Galactic Centre–Sun line is  $20^\circ$  (see Fig. 1).

**Number of spiral arms** Drimmel (2000) used *K*-band photometry of the Galactic plane to conclude that the Milky Way contains two spiral arms. On the other hand, Vallée (2002) reviewed a number of studies about the spiral structure of the Galaxy – mostly based on young stars, gas and dust – and he concluded that the best overall fit is provided by a four-armed spiral pattern. Given this discrepancy, we carry out simulations with  $m = 2$  or 4 spiral arms.

**Amplitude and strength of the spiral arms** We used the amplitude of the spiral arms from the Locus 2 model in Antoja et al. (2011), which is between  $650$  and  $1100 \text{ km}^2 \text{ s}^{-2} \text{ kpc}^{-1}$ . The strength of the spiral arms (as defined in section 5 of Antoja et al. 2011) corresponding to this range of amplitudes is between  $0.029$  and  $0.05$ . We however explored the motion of the Sun for amplitudes of up to  $1300 \text{ km}^2 \text{ s}^{-2} \text{ kpc}^{-1}$  ( $\epsilon \sim 0.06$ ) in a two-armed spiral structure.

**Other parameters** We also use the value of the locus 2 model of Antoja et al. (2011) for the pitch angle ( $i$ ) and scalelength ( $R_\Sigma$ ) of the spiral perturbation. These values are listed in Table 1.

**Transient spiral structure** Several theoretical studies support the idea that spiral arms in galaxies are transient structures (Sellwood & Binney 2002; Sellwood 2011). Nevertheless, Fujii et al. (2011) found that spiral arms in pure stellar discs can survive for more than 10 Gyr when a sufficiently large number of particles ( $\sim 10^7$ ) is used in the simulations. In this work, we use only static spiral structure.

**Multiple spiral patterns** Lépine et al. (2011a) have argued that the corotation radius of the spiral arms is located at solar radius, i.e. at  $R = 8.4 \text{ kpc}$ ; however, based on the orbits of the Hyades and coma Berenices moving groups, Quillen & Minchev (2005) concluded that the 4:1 inner Lindblad resonance of the spiral arms is located at the solar position, placing the corotation resonance at around 12 kpc. To reconcile the uncertainty in the location of the coronation resonance of the spiral structure, Lépine et al. (2011b) suggested the existence of multiple spiral arms with different pattern speeds in the Galaxy. While the main grand-design spiral pattern has its corotation at 8.4 kpc, an outer  $m = 2$  pattern would have its corotation resonance at about 12 kpc, with the 4:1 inner Lindblad resonance at the position of the Sun. These multiple spiral patterns have been observed in *N*-body simulations (see e.g. Quillen et al. 2011).

In this work, we also consider a superposition of spiral patterns as suggested by Lépine et al. (2011b) to study the motion of the Sun in the Galaxy.

### 3 THE AMUSE FRAMEWORK

AMUSE, the Astrophysical MULTipurpose Software Environment (Portegies Zwart et al. 2013), is a framework implemented in PYTHON in which different astrophysical simulation codes can be coupled to evolve complex systems involving different physical processes. For example, one can couple an *N*-body code with a stellar evolution code to create an open cluster simulation in which both gravitational interactions and the evolution of the stars are included. Currently, AMUSE provides interfaces to codes for gravitational dynamics, stellar evolution, hydrodynamics and radiative transfer.

AMUSE is used by writing PYTHON scripts to access all the numerical codes and their capabilities. Every code incorporated in AMUSE can be used through a standard interface which is defined depending on the domain of the code. For instance, a gravitational dynamics

interface defines how a system of particles moves with time and in this case, the user can add or remove particles and update their properties. We created an interface in AMUSE for the Galactic model described in Section 2. For details about how to use AMUSE, we refer the reader to Portegies Zwart et al. (2013) and Pelupessy et al. (2013). More information can also be found at <http://amusecode.org>.

The computation of the stellar motion due to an external gravitational field can be done in AMUSE through the BRIDGE (Fujii et al. 2007) interface. This code uses a second-order Leapfrog method to compute the velocity of the stars due to the gravitational field of the Galaxy. All these computations are performed in an inertial frame. Given that the potentials of the bar and spiral arms are defined to be time independent in a reference system that corotates either with the bar or with the spiral arms, we modified BRIDGE to compute the position and velocity of the Sun in one of such non-inertial frames. Moreover, since the time symmetry of the second-order Leapfrog is no longer valid in a rotating frame, we need to use a higher order scheme. These modifications resulted in a new interface called ROTATING BRIDGE. This code can also be used to perform self-consistent *N*-body simulations of stellar clusters that also respond to the gravitational non-static force from their parent galaxies. In these simulations, the internal cluster effects like self-gravity and stellar evolution can be taken into account. In Appendix A, we derive the equations of motion for the ROTATING BRIDGE for a single particle and its generalization to a system of self-interacting particles. We also show the accuracy of this code under different Galactic parameters.

### 4 BACK-TRACING THE SUN'S ORBIT

Contrary to the epicyclic trajectories that stars follow when they move under the action of an axisymmetric potential, the orbits of stars become more complicated when the gravitational fluctuations generated by the central bar and spiral arms are taken into account, specially where chaos might be important. In chaotic regions, small deviations in the initial position and/or velocity of stars produce significant variations in their final location. Hence, in order to determine the birth place of one star, it is necessary to use a precise numerical code able to resolve the substantial and sudden changes in acceleration that such star experiments. Additionally, it is necessary to compute its orbit backwards in time by using a sampling of positions and velocities around the star's current (uncertain) location in phase space. With this last procedure, we get statistical information about the region in the Galaxy where the star might have been born. We follow this methodology to find the most probable birth radius and velocity of the Sun to infer whether or not it has radially migrated during its lifetime. To ensure numerical accuracy in the orbit integration, we used a sixth-order Leapfrog in the ROTATING BRIDGE with a time step of 0.5 Myr. This choice leads to a fractional energy error of the order of  $10^{-10}$  (see Section A1).

As a first step, we generate 5000 random positions and velocities which are within the measurement uncertainties from the current Galactocentric position and velocity of the Sun ( $\mathbf{r}_\odot$ ,  $\mathbf{v}_\odot$ ). This selection was made from a 4D normal distribution centred at ( $\mathbf{r}_\odot$ ,  $\mathbf{v}_\odot$ ) with standard deviations ( $\sigma$ ) corresponding to the measured errors in these coordinates. We assume that the Sun is currently located at:  $\mathbf{r}_\odot = (-R_\odot, 0) \text{ kpc}$ ; where the distance of the Sun to the Galactic Centre is  $R_\odot \pm \sigma_R = 8.5 \pm 0.5 \text{ kpc}$ . The uncertainty in  $y_\odot$  is set to zero as the Sun is by definition located on the *x*-axis of the Galactic reference frame.

Since we consider the motion of the Sun only on the Galactic plane, the velocity of the Sun is  $\mathbf{v}_\odot = (U_\odot, V_\odot)$ , where

$$U_\odot \pm \sigma_U = 11.1 \pm 1.2 \text{ km s}^{-1}$$

$$V_\odot \pm \sigma_V = (12.4 + V_{\text{LSR}}) \pm 2.1 \text{ km s}^{-1}. \quad (5)$$

The vector  $(11.1 \pm 1.2, (12.4 \pm 2.1) \text{ km s}^{-1})$  is the peculiar motion of the Sun (Schönrich, Binney & Dehnen 2010) and  $V_{\text{LSR}}$  is the velocity of the local standard of rest which depends on the Galactic parameters that are listed in Table 1. We use the conventional Galactocentric Cartesian coordinate system. This means that translated to a Sun-centred reference frame the  $x$ -axis points towards the Galactic Centre, the  $y$ -axis in the direction of Galactic rotation and the  $z$ -axis completes the right-handed coordinate system.

Recently Bovy et al. (2012) found an offset between the rotational velocity of the Sun and  $V_{\text{LSR}}$  of  $26 \pm 3 \text{ km s}^{-1}$ , which is larger than the value measured by Schönrich et al. (2010). We also use this value to trace back the Sun's orbit.

In Fig. 1, we show the configuration of the Galactic potential at the beginning of the backward integration in time. Since it is unknown how spiral arms are oriented with respect to the bar at the centre of the Galaxy, we assume that they start at the edges of the bar. The blue circle in this figure represents the current location of the Sun. The line from the Sun to the Galactic Centre makes an angle of  $20^\circ$  with the semimajor axis of the bar. In the small plot located at the left-hand top of Fig. 1, we show the distribution of the 5000 positions in cylindrical radius  $R$ .

Each of the 5000 positions and velocities that were generated from the 4D normal distribution are used to construct a set of present-day phase-space vectors with (cylindrical) coordinates:  $(R_p, \varphi_p, v_{R_p}, v_{\varphi_p})_k; k = 1, \dots, 5000$  (note that  $\varphi_p$  is fixed at  $\pi$ ). The Sun is then located at each of these vectors and its orbit is computed backwards in time until 4.6 Gyr have elapsed. Before starting the integration, we reversed the velocity components of the Sun as well as the direction of rotation of the bar and spiral arms.<sup>2</sup>

After integrating the orbit of the Sun backwards in time, we obtain a sample of birth phase-space coordinates  $(R_b, \varphi_b, v_{R_b}, v_{\varphi_b})_k; k = 1, \dots, 5000$ . The distributions of present-day and birth phase-space coordinates then allow us to study the past motion of the Sun and infer whether or not it has migrated during its lifetime.

To take the uncertainties on the Galactic model into account, we also varied the bar and spiral arm parameters according to the values listed in Table 1. For a subset of the Galactic model parameters, we verified that 5000 birth phase-space coordinates are a representative number for sampling the position and velocity of the Sun 4.6 Gyr ago. By means of the Kolmogorov–Smirnov test, we found that the distribution of positions and velocities of the Sun after integrating its orbit backwards in time, is the same when  $k = 5000, 10\,000$  or  $20\,000$ . Depending on the Galactic parameters, the  $p$ -value from the test is between 0.2 and 0.98.

## 5 RESULTS

For every choice of bar and spiral arm parameters, we have the distribution of the present-day phase-space coordinates of the Sun  $p(\mathbf{r}_p, \mathbf{v}_p)$  and of the Sun's phase-space coordinates at birth  $p(\mathbf{r}_b, \mathbf{v}_b)$ . The amount of radial migration experienced by the Sun during its

motion through the Galaxy can be obtained from the probability distribution  $p(R_p - R_b)$  (referred to below as the 'migration distribution') of the difference in the radial distance between the present day and birth locations of the Sun. We use the median of the distribution to decide whether or not the Sun has migrated a considerable distance during its lifetime.

- (i) Median  $p(R_p - R_b) > d_m$ : the Sun migrated from inner regions of the Galactic disc to  $R_\odot$  (migration from inside-out).
- (ii) Median  $-d_m \leq p(R_p - R_b) \leq d_m$ : the Sun has not migrated
- (iii) Median  $p(R_p - R_b) < -d_m$ : the Sun migrated from outer regions of the Galactic disc to  $R_\odot$  (migration from outside-in).

The parameter  $d_m$  indicates when the value of  $R_p - R_b$  is considered to indicate a significant migration of the Sun within the Galaxy. We derive the value of  $d_m$  by considering the distribution  $p(R_p - R_b)$  for the case of a purely axisymmetric Galaxy, in which case for the Sun's orbital parameters the migration should be limited. The migration distribution for this case is shown in Fig. 2. From this distribution, it can be seen that for the axisymmetric case indeed the Sun migrates only little on average ( $\sim 0.6 \text{ kpc}$ ) and that the maximum migration distance is about  $1.7 \text{ kpc}$  (note that  $p(R_p - R_b) = 0$  for  $R_p - R_b \lesssim -1.7 \text{ kpc}$ ). Based on this result, we use  $d_m = 1.7 \text{ kpc}$  in the discussions of the results below. Considering changes in the Sun's radial distance larger than  $1.7 \text{ kpc}$  as significant migration is consistent with the estimates of the Sun's migration made by Wielen (1996) and Minchev et al. (2013).

The value of the median of  $p(R_p - R_b)$  is not enough to characterize this probability distribution which is often multimodal (see top panel of Fig. 2) and we thus introduce the following quantities:

$$P_{i \rightarrow o} = \int_{d_m}^{\infty} p(R_p - R_b) d(R_p - R_b)$$

$$P_{o \rightarrow i} = \int_{-\infty}^{-d_m} p(R_p - R_b) d(R_p - R_b), \quad (6)$$

where  $P_{i \rightarrow o}$  is the probability that the Sun has experienced considerable migration from the inner regions of the Galactic disc to its present-day position, while  $P_{o \rightarrow i}$  is the probability that the Sun has significantly migrated in the other direction. One of the aims of our study is to find Milky Way potentials for which the above probabilities are substantial, thus indicating that the Sun has likely migrated a considerable distance over its lifetime.

We also characterize the width of the distribution  $p(R_p - R_b)$  through the so-called Robust Scatter Estimate (RSE) (Lindgren et al. 2012) which is defined as  $\text{RSE} = 0.390152 \times (P90 - P10)$ , where  $P10$  and  $P90$  are the 10th and 90th percentiles of the distribution, and the numerical constant is chosen to make the RSE equal to the standard deviation for a Gaussian distribution.

The orbit integrations were carried out by using the peculiar velocity of the Sun inferred by Schönrich et al. (2010), unless otherwise stated.

### 5.1 Radial migration of the Sun as a function of bar parameters

In order to study the radial migration of the Sun under the variation of mass and pattern speed of the bar, we fixed the amplitude, pattern speed and number of spiral arms such that they have little effect on the Sun's orbit. We chose the values:  $A = 650 \text{ km}^2 \text{ s}^{-2} \text{ kpc}^{-1}$ ,  $\Omega_{\text{sp}} = 20 \text{ km s}^{-1} \text{ kpc}^{-1}$  and  $m = 2$ . With these values of amplitude and pattern speed, we produce spiral arms with a strength at the

<sup>2</sup> The convention used in the ROTATING BRIDGE is right-handed; hence, for the backward integration in time the pattern speed of the bar and spiral arms are positive.

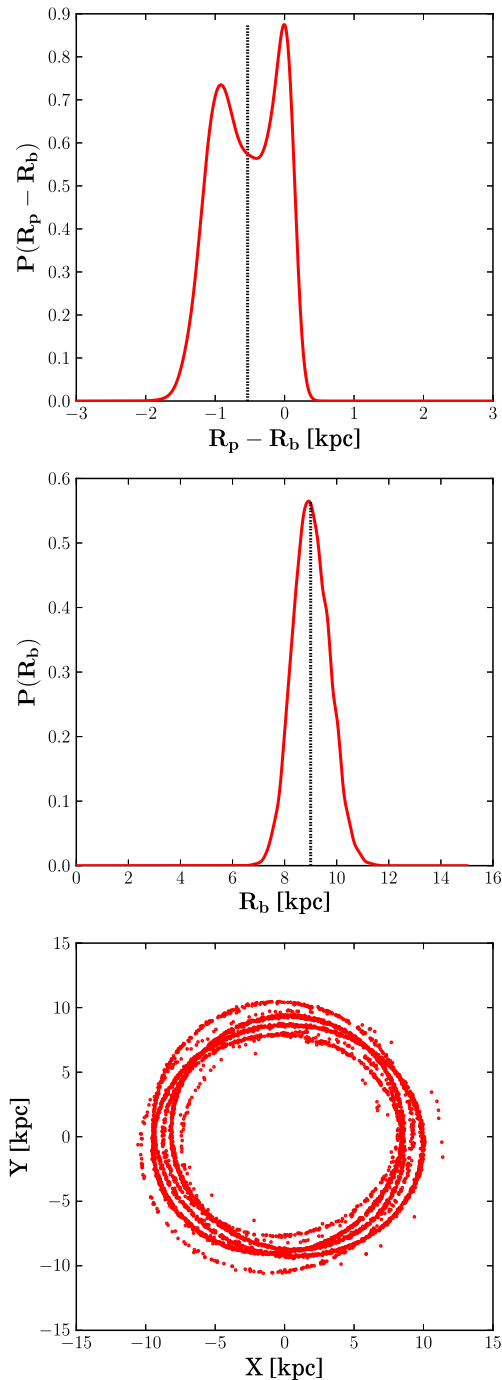


**Figure 2.** Results of the back-tracing of the Sun’s orbit in a purely ax-symmetric Milky Way potential. Top: the migration distribution  $p(R_p - R_b)$ . Middle: distribution of the birth radius of the Sun  $p(R_b)$ . Bottom: the distribution of birth locations of the Sun on the  $xy$ -plane. The dotted black line in the top two panels represents the median of distributions. Note that this is negative for  $p(R_p - R_b)$ , which means that the migration of the Sun is from outer regions of the Galaxy to  $R_\odot$ . The distribution of birth positions of the Sun seen on the  $xy$ -plane suggests that it is not possible to determine the exact formation place of the Sun 4.6 Gyr ago.

lowest limit ( $\epsilon = 0.029$ ) and resonances located in extreme regions of the Galactic disc. The 2:1 inner/outer Lindblad resonance of the spiral arms ( $\text{ILR}_{\text{sp}}$ ,  $\text{OLR}_{\text{sp}}$ ) and the corotation resonance ( $\text{CR}_{\text{sp}}$ ), are located at 1.4, 16 and 10.9 kpc, respectively.

In Fig. 3, we show the median, RSE,  $P_{i-o}$  and  $P_{o-i}$  of the distribution  $p(R_p - R_b)$  as a function of the mass and pattern speed of the bar. The mass of the bar was varied in steps of  $0.02 M_\odot$  and the pattern speed in steps of  $0.5 \text{ km s}^{-1} \text{ kpc}^{-1}$ . The maximum and minimum values of  $M_{\text{bar}}$  and  $\Omega_{\text{bar}}$  were set according to the ranges listed in Table 1. Fig. 3 also shows the position of the 2:1 outer Lindblad resonance of the bar ( $\text{OLR}_{\text{bar}}$ ).

Note that the median of the distribution  $p(R_p - R_b)$  is always negative. This indicates that the migration of the Sun in this case on average is from outer regions of the Galactic disc to  $R_\odot$ . The median of  $p(R_p - R_b)$  is also always lower than 1.08 kpc, independently of the mass and pattern speed of the bar.

On the other hand from the bottom panel of Fig. 3, it is clear that regardless of the mass and pattern speed of the bar, it is unlikely that the Sun has migrated considerably from the inner or outer regions of the Galactic disc to  $R_\odot$ . The low probability of significant radial migration can also be seen in the width of the migration distribution which is always below 0.92 kpc (top-right panel Fig. 3).

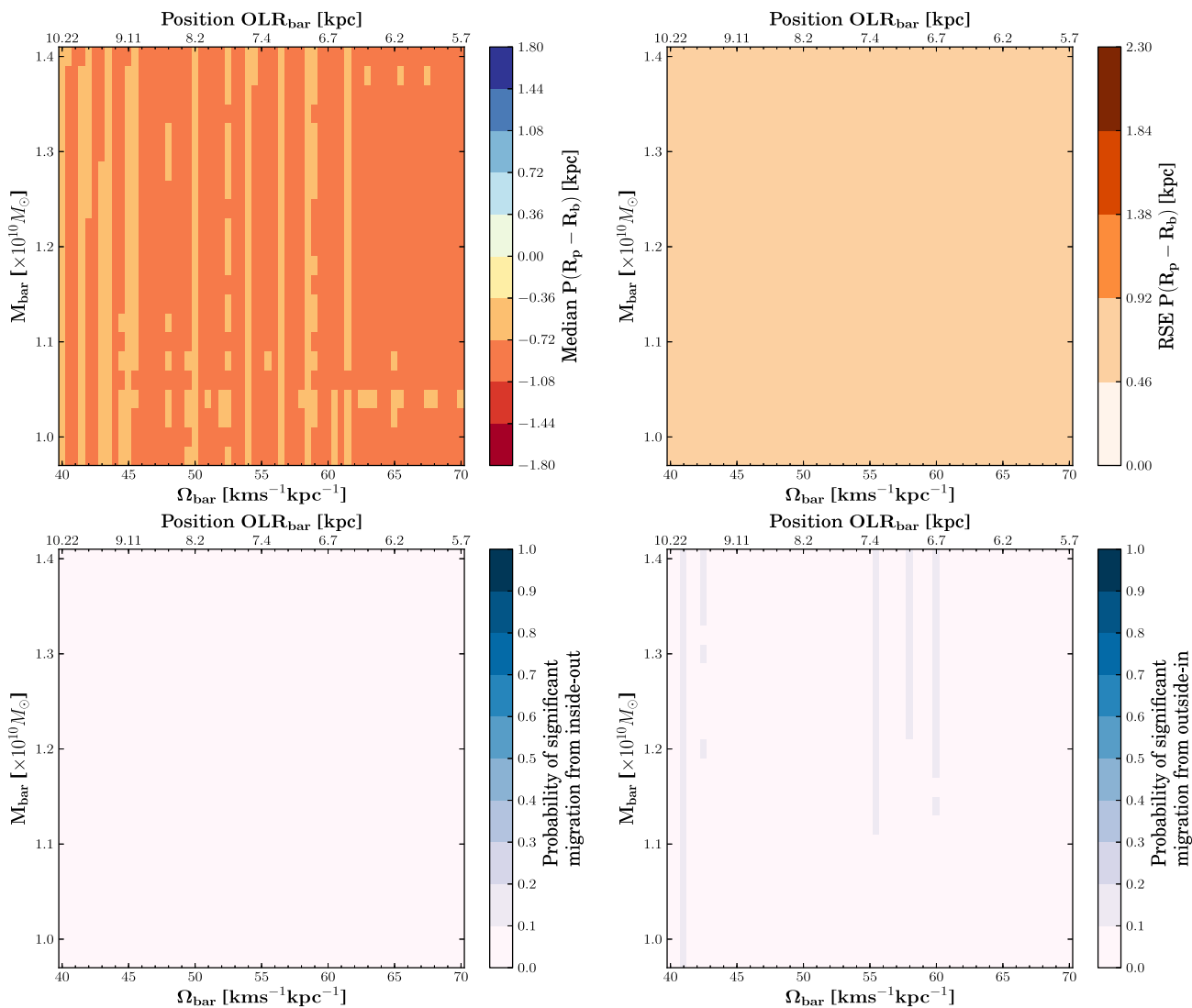
We conclude that the presence of the central bar of the Milky Way does not produce considerable radial migration of the Sun. This result is not surprising, because although the  $\text{OLR}_{\text{bar}}$  has played an important role in shaping the stellar velocity distribution function in the solar neighbourhood (Dehnen 2000; Minchev et al. 2010), the gravitational force produced by the bar falls steeply with radius, reaching about 1 per cent of its total value at  $R_\odot$  (Dehnen 2000). Klačka et al. (2012) studied the motion of the Sun in an analytical model of the Galaxy that considers a multipolar expansion of the bar potential. By assuming the current location of the Sun as  $\mathbf{r}_\odot = (-8, 0, 0) \text{ kpc}$  and  $\mathbf{v}_\odot = (0, 220, 0) \text{ km s}^{-1}$ , they found that the central bar of the Galaxy does not generate considerable radial migration of the Sun if spiral arms are not considered, changing the Galactocentric distance of the Sun only 1 per cent from its current value  $R_\odot$ . We find more than 1 per cent change in radius because we take into account the potential of the spiral arms in the Galactic model.

Fig. 4 shows the distributions  $p(R_p - R_b)$  and  $p(R_b)$  for a choice of bar parameters. In this specific case the median of  $p(R_p - R_b)$  is  $-0.83 \text{ kpc}$ , which means that the birth radius of the Sun is around 9.3 kpc. From the distribution of Sun’s possible birth positions on the  $xy$ -plane (bottom panel Fig. 4), it is clear that even for this smooth and static potential only the birth radius of the Sun can be constrained. The uncertainty in  $\varphi$  for the Sun’s birth location is caused by the uncertainty in the present-day phase-space coordinates of the Sun.

In this section, we have simulated the radial migration of the Sun as a function of mass and pattern speed of the bar. We find no significant migration. In the next section, we study the motion of the Sun when the parameters of the spiral arms are varied.

## 5.2 Radial migration of the Sun as a function of spiral arm parameters

In this section, we study the effects of the spiral structure on the radial migration of the Sun and thus keep fixed the mass and pattern speed of the bar. We chose the lowest limit for the bar mass  $M_{\text{bar}} = 9.8 \times 10^9 M_\odot$ . The pattern speed of the bar was set to be  $\Omega_{\text{bar}} = 40 \text{ km s}^{-1} \text{ kpc}^{-1}$ . With this value, the resonances of the bar are located at extreme regions in the Galactic disc, in particular  $\text{OLR}_{\text{bar}}$  which is at 10.2 kpc. In Section 5.2.1 and 5.2.2, we explore the effects of the amplitude,  $\text{CR}_{\text{sp}}$  location and number of spiral arms on the radial migration of the Sun.



**Figure 3.** Top: median and RSE of the migration distribution  $p(R_p - R_b)$  as a function of the mass and pattern speed of the bar. Negative values in the median indicate migration from outer regions of the Galactic disc to  $R_{\odot}$ , while positive values indicate migration from inner parts to  $R_{\odot}$ . The position of the bar’s outer Lindblad resonance,  $\text{OLR}_{\text{bar}}$ , with respect to the Galactic Centre is also shown. For this set of simulations, the position of  $\text{CR}_{\text{sp}}$  is fixed at 10.9 kpc. Bottom:  $P_{i-o}$  and  $P_{o-i}$  as a function of the mass and pattern speed of the bar.

### 5.2.1 Effect of two spiral arms

In Fig. 5, we show the characteristics of the migration distribution as a function of the amplitude and pattern speed of two spiral arms. We varied the amplitude in steps of  $50 \text{ km}^2 \text{ s}^{-2} \text{ kpc}^{-1}$  and the pattern speed in steps of  $0.2 \text{ km s}^{-1} \text{ kpc}^{-1}$ . Note that for most of the spiral arm parameters the median of  $p(R_p - R_b)$  is negative, suggesting that the migration of the Sun has been mainly from outer regions of the Galactic disc to  $R_{\odot}$ . If the  $\text{CR}_{\text{sp}}$  is located between 9.0 and 10.6 kpc with respect to the Galactic Centre, the median of  $p(R_p - R_b)$  remains between  $-1.08$  and  $-1.44$  kpc for most of the values of  $A_{\text{sp}}$ . The median of  $p(R_p - R_b)$  can reach values of up to  $-1.80$  kpc if  $A_{\text{sp}} = 1100 \text{ km}^2 \text{ s}^{-2} \text{ kpc}^{-1}$  and  $\Omega_{\text{sp}} = 24.2 \text{ km s}^{-1} \text{ kpc}^{-1}$  ( $\text{CR}_{\text{sp}}$  at 9 kpc). For this latter case, there is a probability between 40 and 50 percent that the Sun has migrated considerably from outer regions of the Galactic disc to its current position (cf. Fig. 5, bottom-right panel).

We also studied the radial migration of the Sun for amplitudes higher than  $1100 \text{ km}^2 \text{ s}^{-2} \text{ kpc}^{-1}$ , up to  $1300 \text{ km}^2 \text{ s}^{-2} \text{ kpc}^{-1}$ . We

found that the migration of the Sun on average is from outer regions of the Galactic disc to  $R_{\odot}$ . The Sun only migrates considerably when  $1200 \leq A_{\text{sp}} \leq 1300 \text{ km}^2 \text{ s}^{-2} \text{ kpc}^{-1}$  and  $\Omega_{\text{sp}} = [21.4, 21.8] \text{ km s}^{-1} \text{ kpc}^{-1}$  ( $\text{CR}_{\text{sp}} \sim 10.23$  kpc). According to the former results and given that the  $\text{OLR}_{\text{bar}}$  is located at 10.2 kpc, the significant radial migration of the Sun occurs when the distance between  $\text{CR}_{\text{sp}}$  and  $\text{OLR}_{\text{bar}}$  is in the range  $[0, 1]$  kpc. An illustration of the migration distribution  $p(R_p - R_b)$  for these higher amplitudes is shown in the first and second rows of Fig. 6.

On the other hand, according to the bottom-left panel of Fig. 5, we find that it is unlikely that the Sun has migrated from inner regions of the Galactic disc to  $R_{\odot}$ .

Other studies have also evaluated the effect of the spiral arms of the Milky Way on the motion of the Sun. Klačka et al. (2012) found that under the simultaneous effect of the central bar and spiral arms, the Sun could experience considerable radial migration when it corotates with spiral arms that have a strength  $\epsilon = 0.06$ . In our simulations this strength corresponds to an amplitude  $A_{\text{sp}} = 1300 \text{ km}^2 \text{ s}^{-2} \text{ kpc}^{-1}$ . According to our simulations,

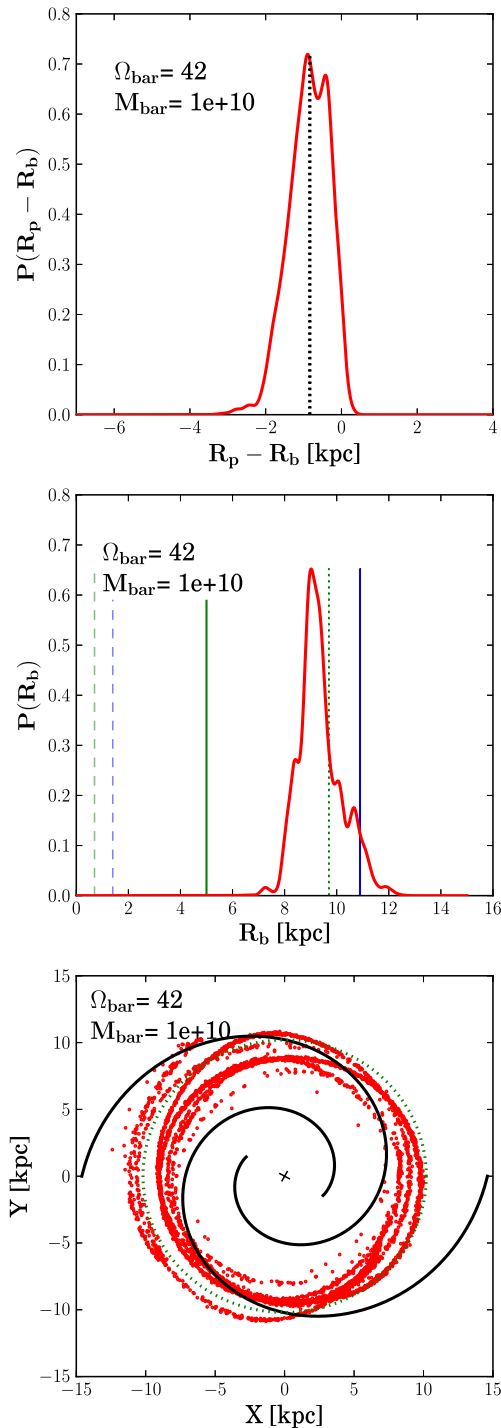


**Figure 4.** Top: distribution function  $p(R_p - R_b)$  for the Galaxy model with weak spiral arms and a central bar. The vertical dotted black line is the median of the distribution. Middle: radial distribution of the birth radius of the Sun  $p(R_b)$  for the same Galactic parameters. The vertical green lines represent the location of the resonances produced by the bar while the blue lines, represent the location of the resonances due to the spiral arms. The dashed, solid and dotted lines represent the 2:1 inner Lindblad (ILR), corotation (CR) and 2:1 outer Lindblad (OLR) resonances, respectively. Hereafter, we will use this same convention. Bottom: distribution of birth positions of the Sun seen on the  $xy$ -plane. The  $OLR_{\text{bar}}$  is shown as the circular dotted green line. We also show the configuration of the spiral arm potential 4.6 Gyr ago.

the Sun experiences considerable radial migration when  $A_{\text{sp}} = 1300 \text{ km}^2 \text{ s}^{-2} \text{ kpc}^{-1}$  and  $\Omega_{\text{sp}} = [21.4, 21.8] \text{ km s}^{-1} \text{ kpc}^{-1}$ ; therefore significant radial migration is found when  $\Omega_{\text{sp}} = 1.2\Omega_{\odot}$ .

By comparing Figs 5 and 3, we can see that a two-armed spiral pattern tends to produce more radial migration on the Sun than the central bar of the Milky Way. Sellwood & Binney (2002), and more recently Minchev & Famaey (2010), found that the larger changes in angular momentum of stars always occur near the corotation resonance, the effect of the outer/inner Lindblad resonances being smaller. Given that in our simulations the motion of the Sun is influenced by the  $CR_{\text{sp}}$  and by the  $OLR_{\text{bar}}$ , it is expected that the spiral arms produce a stronger effect on the Sun's radial migration than the central bar of the Galaxy.

At the top panel of Fig. 6, we show the distributions  $p(R_p - R_b)$  and  $p(R_b)$  for an example of a two-arm spiral arm potential that leads to considerable radial migration of the Sun. In this case the distance between the  $CR_{\text{sp}}$  and  $OLR_{\text{bar}}$  is 0.03 kpc. For this specific set of bar and spiral arm parameters, the Sun could have migrated a distance of 1.8 kpc from the outer regions of the Galactic disc to its current position. Its birth radius would then be around 11 kpc, as also indicated by the distribution  $p(R_b)$ . The projection of the Sun's birth locations in the  $xy$ -plane shows lots of structure, but again only the birth radius can be constrained.

In the second row of Fig. 6, we show the distributions  $p(R_p - R_b)$  and  $p(R_b)$  for a set of spiral arm parameters that produce high dispersion in the migration distribution  $p(R_p - R_b)$ . In this case the Sun does not migrate on average (Median  $p(R_p - R_b) \sim 0$ ). Additionally, as can be observed in the plot on the right, there is a fraction of possible birth radii at the inner regions of the Galactic disc; however, the probability of significant migration from inside-out in this case is only of 10 per cent.

### 5.2.2 Effect of four spiral arms

We also assess the radial migration of the Sun under the action of a Galactic potential composed of four spiral arms. The results are shown in Fig. 7. Note that when  $\Omega_{\text{sp}}$  is between 19 and 22  $\text{km s}^{-1} \text{ kpc}^{-1}$  the radial migration experienced by the Sun is less than 1 kpc. Additionally, when  $CR_{\text{sp}}$  is located between 7.3 and 8.4 kpc, the median of  $p(R_p - R_b)$  is between  $-0.36$  and  $0.36$  kpc (around zero). However, the large width of the distribution leads to probabilities of up to 30 per cent that the Sun has migrated from inner regions of the Galactic disc to its current position. The probability of significant migration in the other direction is up to 20 per cent.

The larger width of  $p(R_p - R_b)$  may be due to the effect of higher order resonances (4:1  $ILR_{\text{sp}}/OLR_{\text{sp}}$ ) on the motion of the Sun. The fact that the width of  $p(R_p - R_b)$  is large for specific four-armed Galactic potentials, means that the migration of the Sun is very sensitive to its birth phase-space coordinates. This effect can be also observed in the third row of Fig. 6, which shows  $p(R_p - R_b)$  and  $p(R_b)$  when the Galactic potential has four spiral arms. In addition, the projection of the possible birth locations on the  $xy$ -plane shows virtually no structure.

By comparing Figs 5 and 7, we can see that unlike the case when the Galactic potential has two spiral arms, the median of  $p(R_p - R_b)$  when  $m = 4$  is not much affected by small separation distances between the  $CR_{\text{sp}}$  and  $OLR_{\text{bar}}$ .

### 5.2.3 Effects of multiple spiral patterns

In addition to evaluating the motion of the Sun in a pure two-armed or four-armed spiral structure, we use a superposition of two



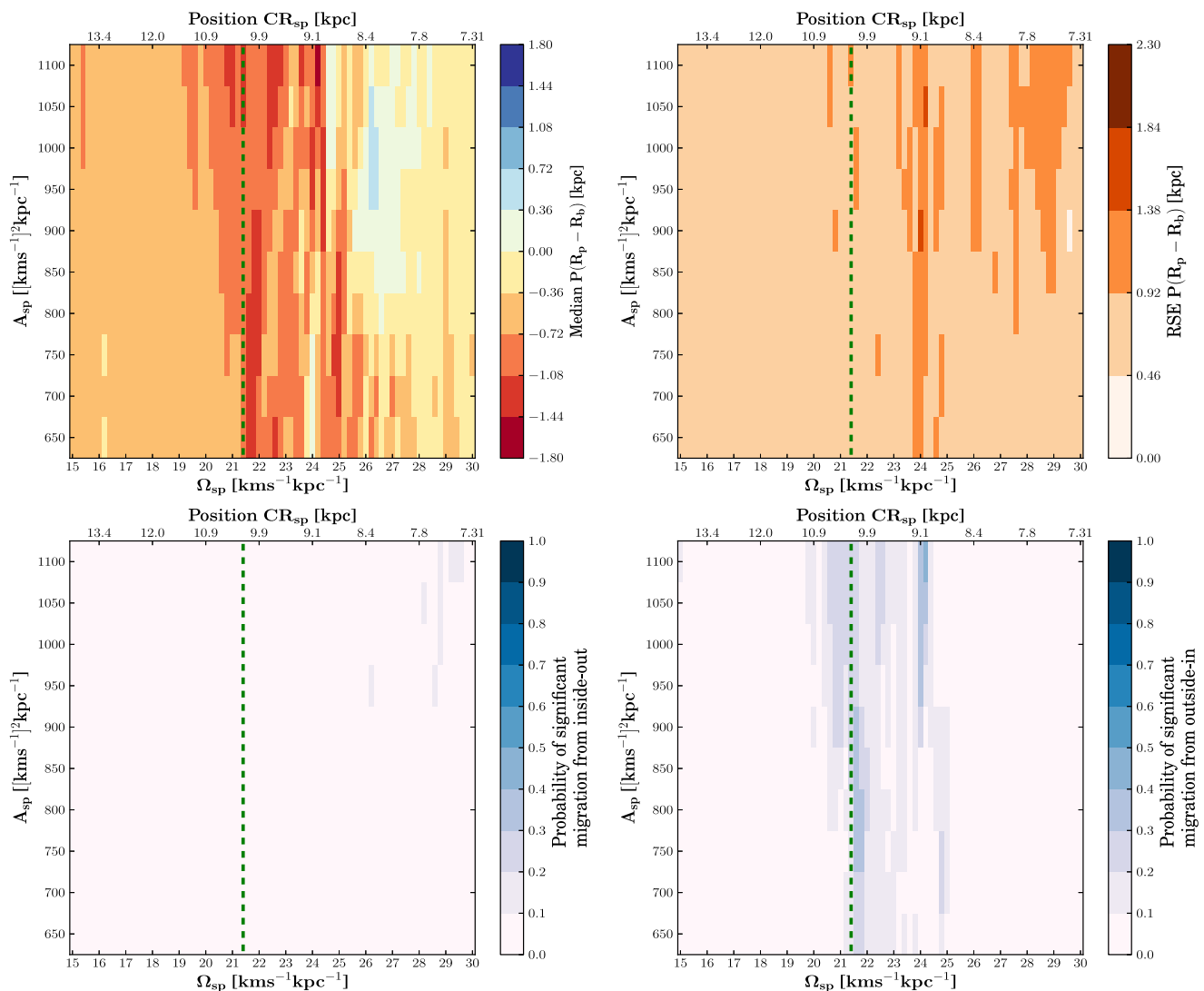


**Figure 5.** Top: median and RSE of the distribution  $p(R_p - R_b)$  as a function of the amplitude and pattern speed of a two-armed spiral structure. The location of the  $CR_{sp}$  with respect to the Galactic Centre is also shown. For this set of simulations, the position of the outer Lindblad resonance of the bar,  $OLR_{bar}$  is fixed at 10.2 kpc and it is shown as the vertical dotted green line. Bottom:  $P_{i-o}$  and  $P_{o-i}$  also as a function of the amplitude and pattern speed of two spiral arms.

spiral arms (2 + 2) with different pattern speeds, such as discussed by Lépine et al. (2011b). We use the same values as Mishurov & Acharova (2011) to set the pitch angles of the multiple spiral patterns in the Milky Way. The parameters of the main spiral structure used in the simulations are:  $A_{sp1} = 650, 1300 \text{ km}^2 \text{ s}^{-2} \text{ kpc}^{-1}$ ;  $i_1 = -7^\circ$  and  $\Omega_{sp1} = 26 \text{ km s}^{-1} \text{ kpc}^{-1}$ . This pattern speed places the  $CR_{sp}$  of the main spiral structure at solar radius. The orientation of the main spiral pattern at the beginning of the simulations is  $20^\circ$ .

The parameters used to model the secondary spiral structure are:  $A_{sp2} = 0.8A_{sp1}$ ;  $i_2 = -14^\circ$  and  $\Omega_{sp2} = 15.8 \text{ km s}^{-1} \text{ kpc}^{-1}$ . This pattern speed places the  $CR_{sp}$  of the secondary spiral structure at 13.6 kpc and the 4:1  $ILR_{sp}$  at 7.8 kpc. The orientation of the secondary spiral arms with respect to the main structure at the beginning of the simulations is  $-200^\circ$ . In addition, we fixed the mass and pattern speed of the bar to  $M_{bar} = 9.8 \times 10^9 M_\odot$  and  $\Omega_{bar} = 40 \text{ km s}^{-1} \text{ kpc}^{-1}$ , respectively.

At the bottom panel of Fig. 6, we show the distributions  $p(R_p - R_b)$  and  $P(R_b)$  when the Galactic potential has multiple

spiral patterns. In this simulation the amplitude of the main spiral structure is  $A_{sp1} = 1300 \text{ km}^2 \text{ s}^{-2} \text{ kpc}^{-1}$ . We used the tangential velocity of the Sun from Bovy et al. (2012). As can be seen, the median of the distribution  $p(R_p - R_b)$  is smaller than 1 kpc, meaning that the migration of the Sun on average is not significant. The birth radius of the Sun is therefore at 8.5 kpc, as can also be seen from the distribution  $P(R_b)$ . The projection of birth locations of the Sun on the  $xy$ -plane suggest that there is some fraction of possible birth radii located at internal regions of the Galactic disc; however, we found that the probability of considerable migration from outer or inner regions to  $R_\odot$  is between 8 and 13 per cent. These probabilities are even smaller when  $A_{sp1} = 650 \text{ km}^2 \text{ s}^{-2} \text{ kpc}^{-1}$ . We obtain the same results when assuming  $V_\odot$  from Schönrich et al. (2010).

In Section 5.2.1, we have shown that the Sun might have experienced considerable migration in the Galaxy if the  $CR_{sp}$  is separated from the  $OLR_{bar}$  by a distance smaller than 1.1 kpc. In the next section, we explore in more detail the effect of the bar-spiral arm resonance overlap on the motion of the Sun.

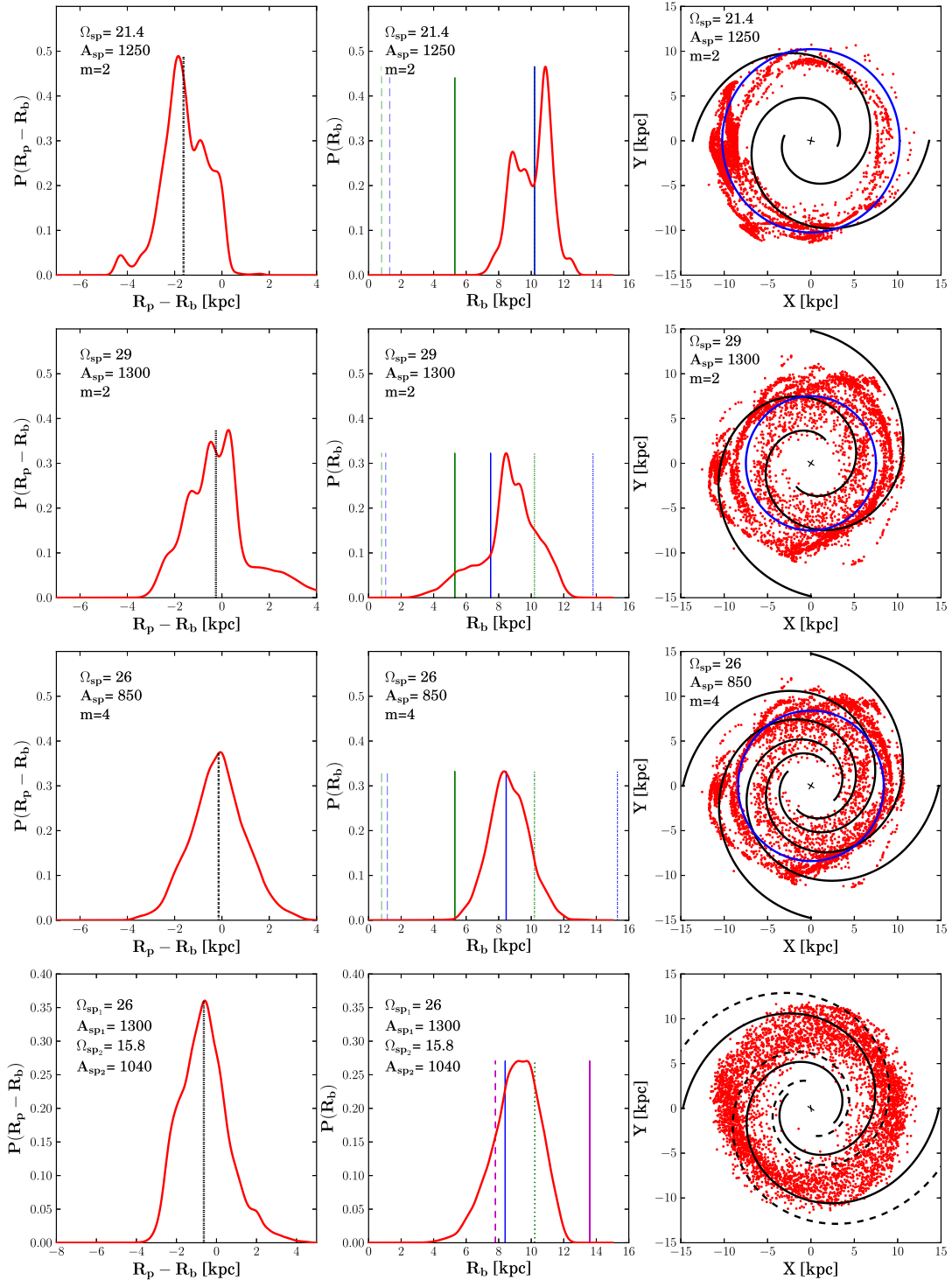


**Figure 6.** Left: migration distribution  $p(R_p - R_b)$ . Middle: distribution of possible Sun's birth radii  $P(R_b)$ . Right: projection on the  $xy$ -plane of the possible birth radii of the Sun. A specific combination of bar and spiral arm parameters are used. In the first and second rows, the Galactic potential has two spiral arms. In the third row, the Galactic potential has four spiral arms. In the bottom panel, we use a superposition of two spiral arms ( $2 + 2$ ) with different pattern speeds. The pattern speed and mass of the bar are fixed to  $\Omega_{\text{bar}} = 40 \text{ km s}^{-1} \text{ kpc}^{-1}$  and  $M_{\text{bar}} = 9.8 \times 10^9 M_{\odot}$ , respectively. The vertical dotted black line in the panels on the left is the median of the distribution  $p(R_p - R_b)$ . The same line styles as in Fig. 3 are used to indicate the resonances due to the bar and spiral arms in the panel on the middle. In the same panel at the bottom, the dashed and solid magenta lines correspond to the  $\text{ILR}_{\text{sp}}$  and  $\text{CR}_{\text{sp}}$  of the secondary spiral structure. The blue circle in the panels on the right in the first three rows represents the position of  $\text{CR}_{\text{sp}}$ , which is located from top to bottom at 9.9, 7.6 and 8.4 kpc, respectively. The  $\text{CR}_{\text{sp}}$  due to the multiple spiral patterns are not shown in the plot on the bottom. In the right-hand panel, we also show the configuration of the spiral arm potential 4.6 Gyr ago. The dashed black line in the figure of the bottom represents the secondary spiral structure.

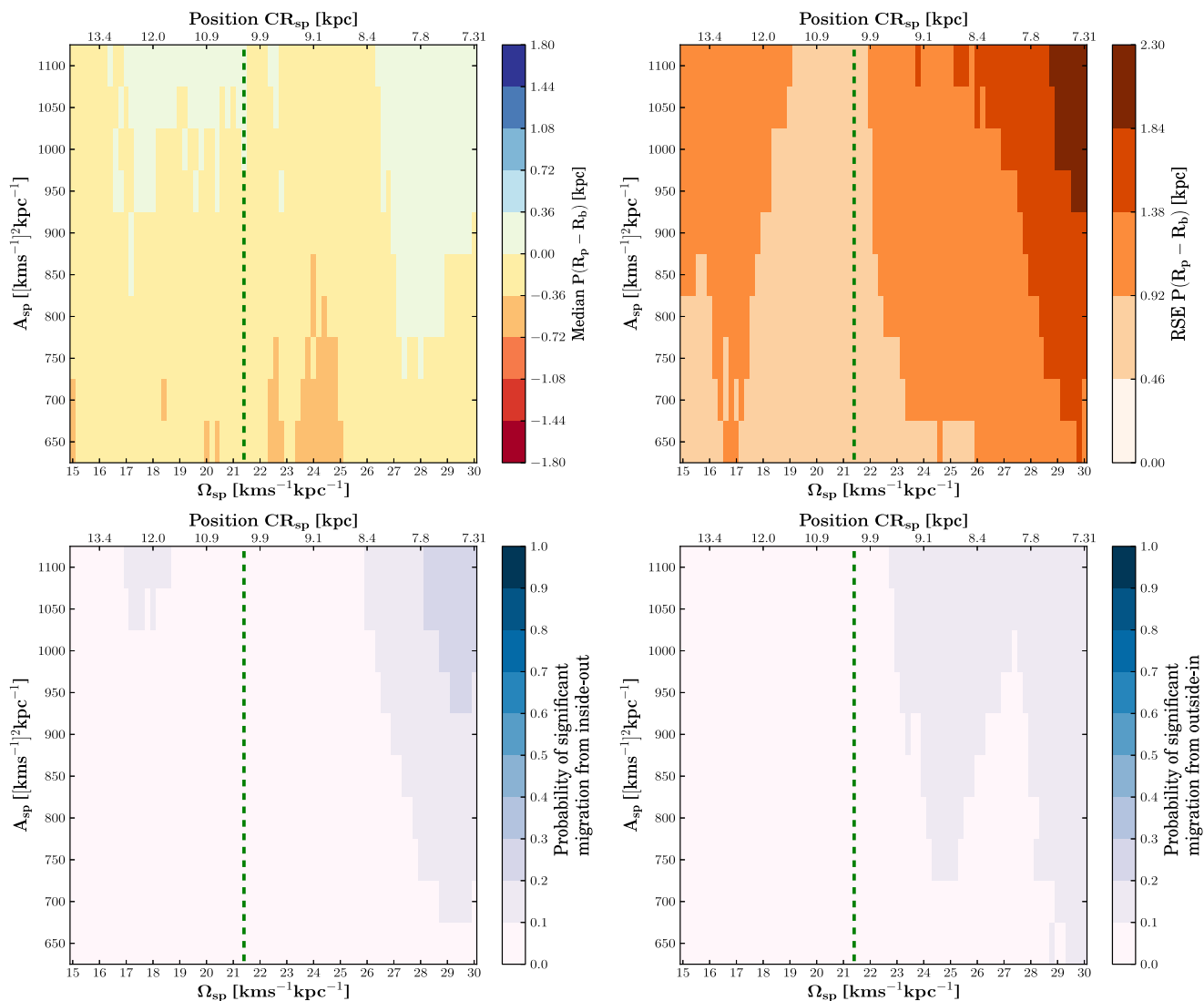


**Figure 7.** Top: median and RSE of the distribution  $p(R_p - R_b)$  as a function of the amplitude and pattern speed of a four-armed spiral structure. The location of the  $\text{CR}_{sp}$  with respect to the Galactic Centre is also shown. For this set of simulations, the position of the  $\text{OLR}_{bar}$  is fixed at 10.2 kpc and it is shown as the vertical dotted green line. Bottom:  $P_{i-o}$  and  $P_{o-i}$  also as a function of the amplitude and pattern speed of four spiral arms.

### 5.3 Radial migration of the Sun in the presence of the bar-spiral arm resonance overlap

It has been demonstrated by Minchev & Famaey (2010) and Minchev et al. (2011) that the dynamical effects of overlapping resonances from the bar and spiral arms provide an efficient mechanism for radial migration in galaxies. Depending of the strength of the perturbations, radial mixing in Galactic discs proceeds up to an order of magnitude faster than in the case of transient spiral arms. Given that the solar neighbourhood is near to the  $\text{OLR}_{bar}$  and that the Sun is located approximately at 1 kpc from  $\text{CR}_{sp}$  (Acharova, Mishurov & Rasulova 2011), it is of interest to study the radial migration that the Sun might have experienced under the influence of the spiral-bar resonance overlap.

It is well known that galactic discs rotate differentially. However, the gravitational non-axisymmetric perturbations such as the central bar and spiral arms, rotate as rigid bodies. In consequence, stars at different radii will experience different forcing due to these non-axisymmetric structures (Minchev & Famaey 2010). There are specific locations in the Galactic disc where stars are in resonance

with the perturbations. One is the corotation resonance, where stars move with the same pattern speed of the perturber, and the Lindblad resonances, where the frequency at which a star feels the force due to the perturber coincides with its epicyclic frequency  $\kappa$ . Depending on the position of the star, inside or outside from the corotation radius, it can feel the Inner or Outer Lindblad resonances.

In Fig. 8, we show the resonances of second multiplicity (for  $m = 2$ ) in a galactic disc. The green and red shaded regions correspond to the accepted values of the pattern speed of the bar and spiral arms of the Milky Way within the uncertainties. As can be seen,  $\Omega_{bar}$  and  $\Omega_{sp}$  only allow certain combinations of resonance overlaps. For the case of two spiral arms, only the overlap of the  $\text{OLR}_{bar}$  and  $\text{CR}_{sp}$  is possible.<sup>3</sup> Hereafter we refer to this resonance overlap as the  $\text{OLR/CR}$  overlap.

To explore the motion of the Sun in the presence the overlapping of resonances, we vary the pattern speed of the bar and spiral arms

<sup>3</sup> For  $m = 2$ , we do not take into account second-order resonances, i.e. 4:1 ( $\text{ILR}_{bar, sp}, \text{OLR}_{bar, sp}$ ).

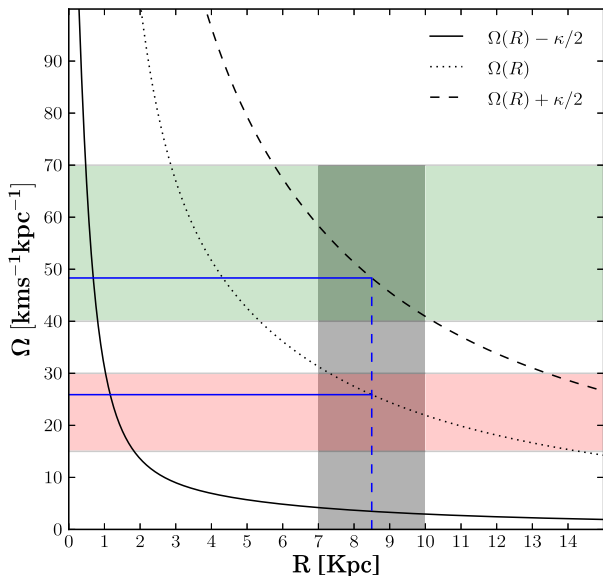


**Figure 8.** Resonances of second multiplicity (for  $m = 2$ ) in galactic discs. The inner and outer Lindblad resonances (ILR, OLR) are along the solid and dashed black lines. They are given by:  $\Omega(R) \pm \kappa/2$ , where the minus (plus) sign corresponds to the ILR (OLR). The corotation resonance (CR) is along the dotted black line and it is given by:  $\text{CR} = \Omega(R)$ . The shaded green region corresponds to the pattern speed of the bar within its uncertainty. The shaded red region corresponds to the pattern speed of spiral arms within its uncertainty. Note that  $\Omega_{\text{bar}}$  and  $\Omega_{\text{sp}}$  only allow the overlapping between the Outer Lindblad resonance of the bar (OLR<sub>bar</sub>) with the corotation of spiral arms (CR<sub>sp</sub>). We refer this resonance overlap as OLR/CR overlap. The grey shaded region is the location of the OLR/CR overlap in the simulations. The blue lines show how we set  $\Omega_{\text{bar}}$  and  $\Omega_{\text{sp}}$  to generate the OLR/CR overlap at some desired position.

such that the OLR/CR overlap is located at different positions in the disc, between 7 and 10.2 kpc from the Galactic Centre, as indicated by the vertical grey shaded line in Fig. 8. In our simulations, we varied the location of the OLR/CR overlap every 0.1 kpc. The amplitude of the spiral arms and the mass of the bar were also varied.

In Fig. 9, we show the median of  $p(R_p - R_b)$  as a function of the position within the Galactic disc of the OLR/CR overlap. From left to right, the amplitude of spiral arms increases; from top to bottom, the mass of the bar is  $9.8 \times 10^9$  and  $1.3 \times 10^{10} M_\odot$ . Note that regardless of the amplitude of the spiral arms or the mass of the bar, when the OLR/CR overlap is located at distances smaller than 8.5 kpc, the migration of the Sun is not considerable. In fact, for these cases, the probability that the Sun has migrated significantly in either direction is smaller than 10 per cent (see Fig. 10). In contrast, when the OLR/CR overlap is located at distances larger than 8.5 kpc, the median of the distribution  $p(R_p - R_b)$  is shifted towards negative values, while the probability for considerable migration from the outer disc to  $R_\odot$  goes up reaching values up to 35 per cent. The probability of significant migration from the inner disc to  $R_\odot$  remains low at values of at most a few per cent.

In Fig. 11, we show the migration distribution for an example of a case where the OLR/CR overlap has a strong effect, being located at 9.7 kpc from the Galactic Centre. For this particular case,  $M_{\text{bar}} = 9.8 \times 10^9 M_\odot$  and  $A_{\text{sp}} = 1100 \text{ km}^2 \text{ s}^{-2} \text{ kpc}^{-1}$ . The median of  $p(R_p - R_b)$  is at  $-1.3 \text{ kpc}$  and thus the radius where the Sun was born is around 10 kpc. The latter can also be seen in the distribution  $p(R_b)$ . Note how the distribution of birth positions in the  $xy$ -plane is clustered between the second and third quadrants. This is also seen for other cases, when the OLR/CR overlap is located between 8.5 and 9.5 kpc. However, for different OLR/CR distances the clustering is towards other quadrants in the Galactic

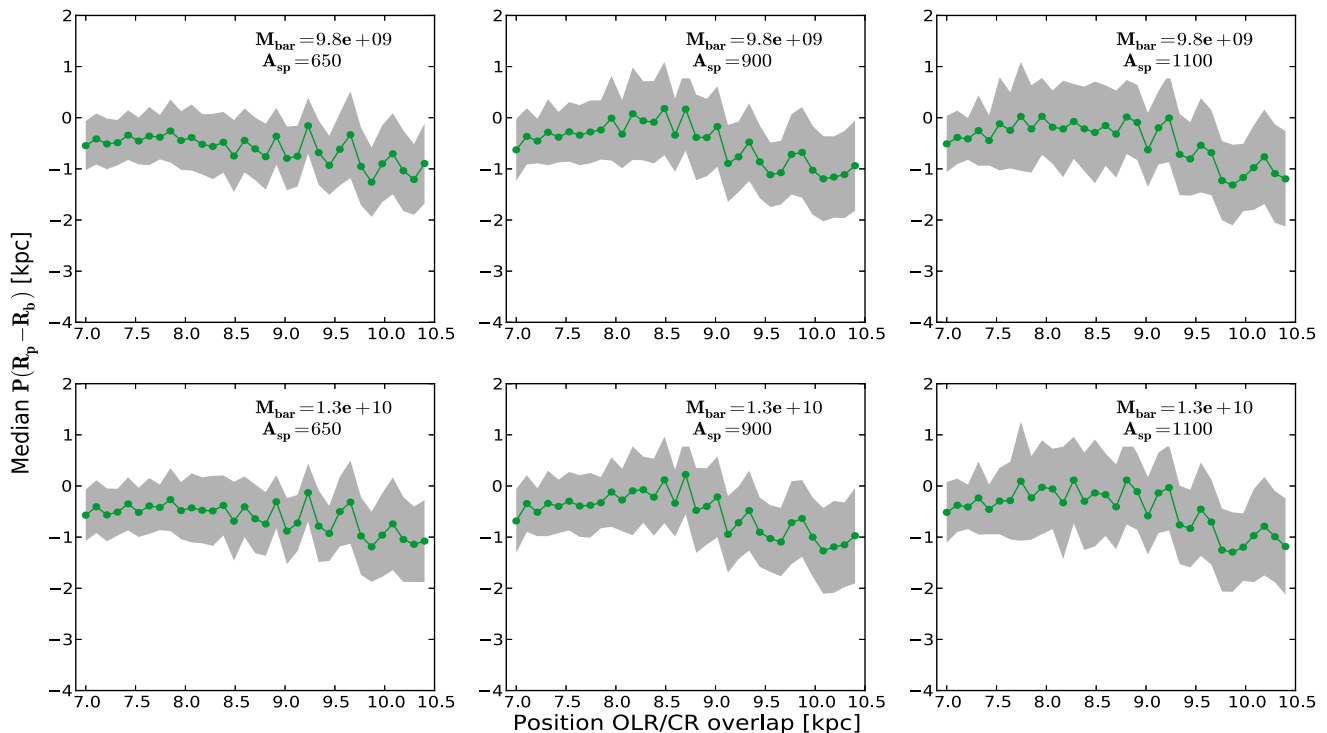


**Figure 9.** Median of the migration distribution  $p(R_p - R_b)$  as a function of the position within the Galactic disc of the OLR/CR overlap. The shaded region corresponds to the RSE of the same distribution. From left to right, the amplitude of the spiral arms,  $A_{\text{sp}}$  takes the values 650, 900 and  $1100 \text{ km}^2 \text{ s}^{-2} \text{ kpc}^{-1}$ . From top to bottom, the mass of the bar,  $M_{\text{bar}}$  is  $9.8 \times 10^9$  and  $1.3 \times 10^{10} M_\odot$ .

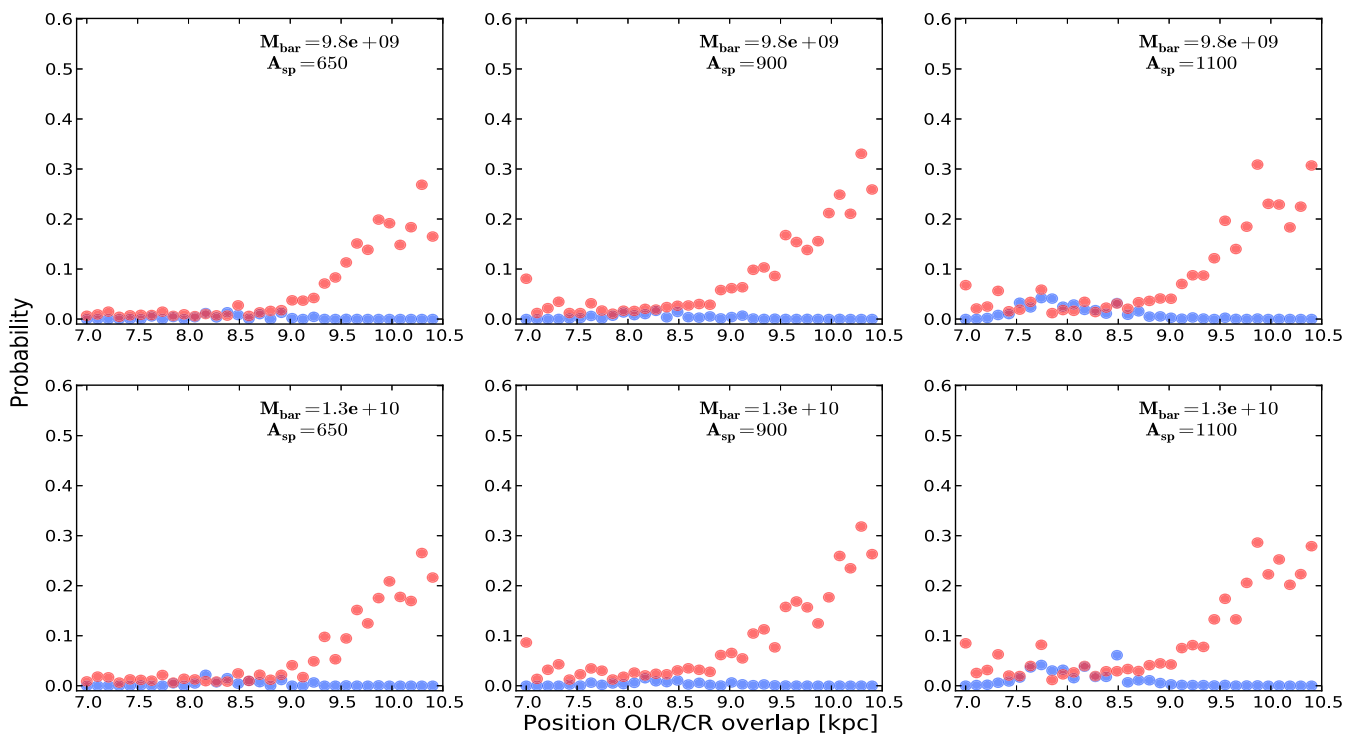


**Figure 10.** Probability of considerable radial migration of the Sun as a function of the location of the OLR/CR overlap. The blue points represent the probability of significant migration of the Sun from inside-out  $P_{i-o}$ , while the red points represent the significant migration from outside-in  $P_{o-i}$ . The mass of the bar and amplitude of spiral arms are the same as in Fig. 9.

plane. Hence, taking the uncertainties in the OLR/CR location into account again only the birth radius of the Sun can be constrained.

#### 5.4 Radial migration of the Sun with higher values of its tangential velocity

In this section, we explore the motion of the Sun backwards in time when assuming the rotational velocity suggested by Bovy et al. (2012). In Fig. 12, we show the median of the distribution  $p(R_p - R_b)$  as a function of the distance between the  $OLR_{bar}$  and  $CR_{sp}$ . For this set of simulations, we fixed the bar parameters to  $M_{bar} = 9.8 \times 10^9 M_{\odot}$  and  $\Omega_{bar} = 40 \text{ km s}^{-1} \text{ kpc}^{-1}$ , respectively. With this pattern speed, the  $OLR_{bar}$  is located at 10.2 kpc with respect to the Galactic Centre. Additionally, the amplitude of the spiral arms is fixed to  $A_{sp} = 1050 \text{ km}^2 \text{ s}^{-2} \text{ kpc}^{-1}$ . We varied the pattern speed of the spiral arms in steps of  $1 \text{ km s}^{-1} \text{ kpc}^{-1}$  within the range listed in Table 1. We used two and four spiral arms. For comparison, we have also plotted the median of the distribution  $p(R_p - R_b)$  when the tangential velocity of the Sun is taken from Schönrich et al. (2010). As can be observed, the migration of the Sun on average is approximately 1 kpc higher when  $V_{\odot}$  is taken from Bovy et al. (2012). In the latter case, the median of the distribution  $p(R_p - R_b)$  is negative for both  $m = 2$  and 4 meaning that the Sun has migrated from outer regions of the Galactic disc to  $R_{\odot}$ . In addition, from the simulations shown at the top panel of Fig. 12, we found that when the  $OLR_{bar}$  and  $CR_{sp}$  are separated by  $\pm 0.2 \text{ kpc}$ , the Sun migrates on average a distance around 2 kpc, placing the Sun's birth place at around 10.5 kpc from the Galactic Centre. For this specific case, we found a probability between 55 and 60 per cent that the Sun has migrated considerably from outer regions of the Galactic disc to its current position. On the other hand, we found unlikely that the Sun has migrated from inner regions of the Galaxy to  $R_{\odot}$ .

Contrary to the two-armed spiral structure, the migration of the Sun on average is not significant when  $m = 4$ , even for small distances between the  $OLR_{bar}$  and  $CR_{sp}$  (see bottom panel Fig. 12). Note that the median of  $p(R_p - R_b)$  is never greater than  $-1.7 \text{ kpc}$ . However, given that the width of the distribution  $p(R_p - R_b)$  is appreciable, specially when  $OLR_{bar} - CR_{sp} \geq 2 \text{ kpc}$ , the probability of considerable migration from inner or outer regions to  $R_{\odot}$  can be of up to 10 or 20 per cent, respectively.

## 6 DISCUSSION

It is well known that the metallicity of the interstellar medium (ISM) depends on time and Galactic radius. Since younger stars formed at the same Galactocentric radius have higher metallicities, the metallicity of the ISM is expected to increase with time. Additionally, it has been established that the metallicity of the ISM decreases with increasing the Galactic radius due to more efficient star formation and enrichment of the ISM in the central regions of galaxies (Daflon & Cunha 2004; Recio-Blanco et al. 2014).

Past studies of the age–metallicity relation in the solar neighbourhood suggested that the Sun is more metal rich by typically 0.2 dex than most stars at its age and Galactocentric orbit (Edvardsson et al. 1993; Holmberg et al. 2009). Hence, from the relationship between metallicity and Galactocentric radius, it is natural to deduce that the Sun might have migrated from the inner regions of the disc to its current position in the Galaxy (Wielen 1996; Minchev et al. 2013). However, if the observations are restricted to stars within a distance of 40 pc from the Sun it seems that its chemical composition is not unusual after all. Fuhrmann (2004) found a sample of 118 thin-disc stars with a mean age of 4.5 Gyr to have a mean metallicity of  $-0.04 \text{ dex}$ . In addition Valenti & Fischer (2005), found a mean metallicity of  $-0.01 \text{ dex}$  in a sample of F, G and K stars

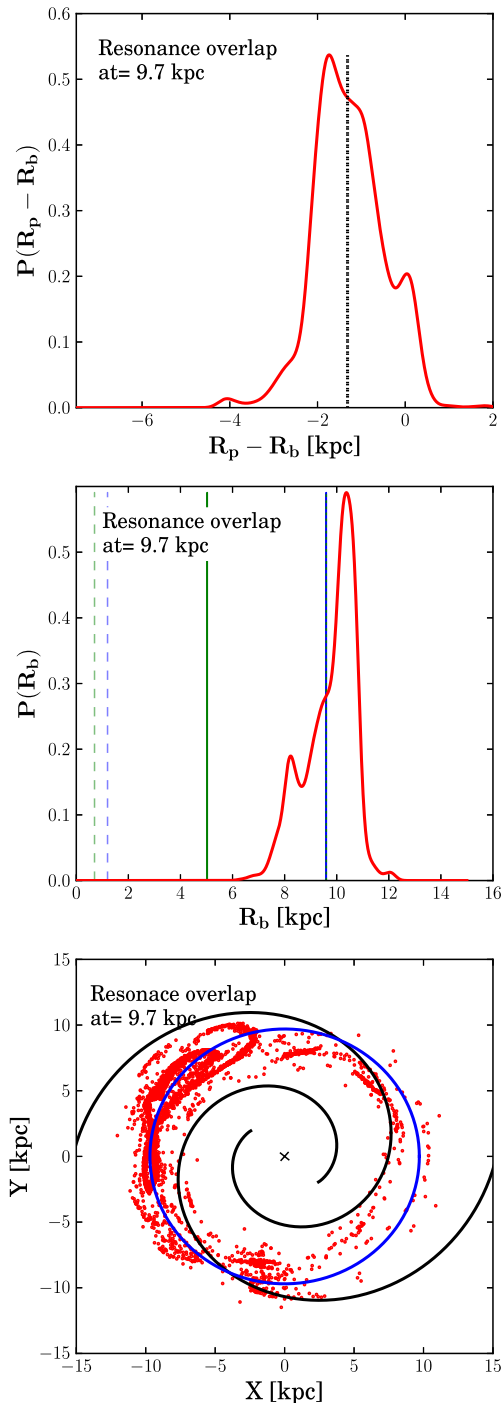


**Figure 11.** Example of the migration distribution for the case of the OLR/CR overlap located at 9.7 kpc from the Galactic Centre. Here  $A_{\text{sp}} = 1100 \text{ km}^2 \text{ s}^{-2} \text{ kpc}^{-1}$  and  $M_{\text{bar}} = 9.8 \times 10^9 M_{\odot}$ . Top: the migration distribution  $p(R_p - R_b)$ . The dotted black line indicates the median of the distribution. Middle: distribution of the birth radius of the Sun  $p(R_b)$ . Bottom: distribution of birth positions of the Sun projected on the  $xy$ -plane. The location of the OLR/CR overlap is indicated by the blue circle. The configuration of the spiral arm potential 4.6 Gyr in the past is also shown.

that were observed in the context of planet search programmes. More recently, Casagrande et al. (2011) found that the peak of the metallicity distribution function of stars in the Geneva–Copenhagen survey (Nordström et al. 2004), is around the solar value. As we

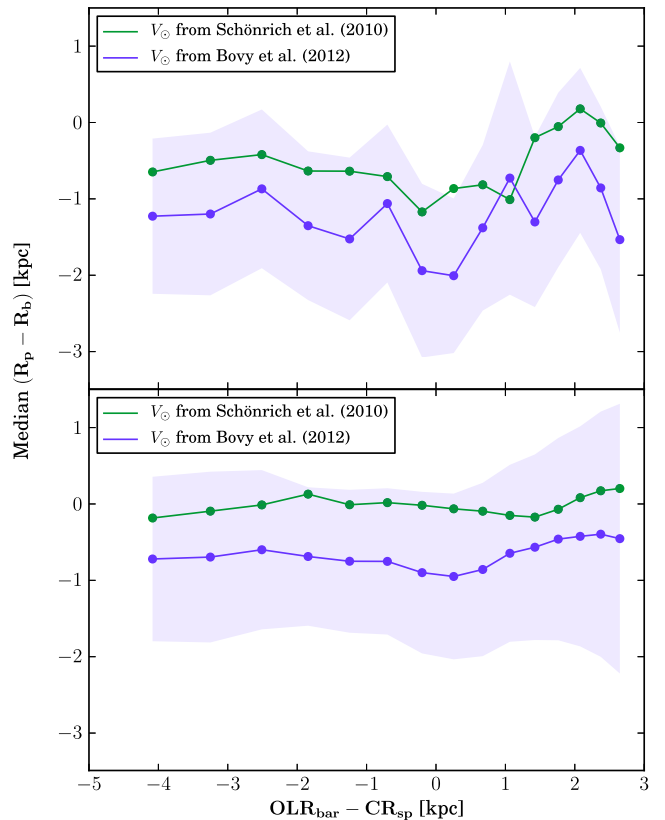


**Figure 12.** Median of the distribution  $p(R_p - R_b)$  as a function of the distance between the  $\text{OLR}_{\text{bar}}$  and  $\text{CR}_{\text{sp}}$ . The green line is the resulting radial migration of the Sun when we assume a tangential velocity of  $12.4 \pm 2.1 \text{ km s}^{-1}$  (Schönrich et al. 2010) in the orbit integration backwards in time. The blue line is the radial migration of the Sun when we assume a tangential velocity of  $26 \pm 3 \text{ km s}^{-1}$  (Bovy et al. 2012). The blue shaded region corresponds to the RSE of  $p(R_p - R_b)$  for this latter case. We used: top – two spiral arms and bottom – four spiral arms.

mentioned in the Introduction, if the Sun is indeed not more metal rich than the stars of its same age and Galactocentric radius it is probable that the Sun has not experienced considerable migration over its lifetime.

Minchev & Famaey (2010) studied the effects of the bar-spiral arm resonance overlap in the solar neighbourhood. They found that a large fraction of stars that were located initially at inner and outer regions of the Galactic disc, ended up at a distance of  $\sim 8 \text{ kpc}$  after 3 Gyr of evolution. This explains the observed lack of a metallicity gradient with age in the solar neighbourhood (Haywood 2008); however, the same simulations show that after 3 Gyr of evolution, the peak of the initial radial distribution of stars that end up at 8 kpc is also around 8 kpc, meaning that most of the stars at solar radius, do not migrate. For their simulations, Minchev & Famaey (2010) modelled the central bar and spiral arms of the Galaxy as non-transient perturbations.

In this study, we find that large radial migration of the Sun is only feasible when the  $\text{OLR}_{\text{bar}}$  is separated from  $\text{CR}_{\text{sp}}$  by a distance less than 1.1 kpc or when these two resonances overlap and are located further than 8.5 kpc from the Galactic Centre. In these cases, we find that the migration of the Sun is always from the outer regions of the Galaxy to  $R_{\odot}$ . When the  $\text{CR}_{\text{sp}}$  is located between 7.3 and 8.4 kpc and the number of spiral arms is four, the Sun migrates on

average little; however, given that the width of the distribution  $p(R_p - R_b)$  can be up to 2.3 kpc, the radial migration of the Sun highly depends on its birth phase-space coordinates. For this latter case, the probability that the Sun has migrated considerably from inner regions of the disc to  $R_\odot$  can be up to 30 per cent. Apart from the very specific cases mentioned above, we found that in general the Sun might have not experienced considerable radial migration from its birth place to its current position in the Galaxy. In the simulations we did not change the Galactic parameters (mass, scalelength) of the axisymmetric components of the Milky Way. Since this is a smooth potential, we do not expect great variations on the solar motion due to the variation of these parameters.

The model that we used for the Milky Way has two restrictions: it does not take into account transient spiral structure and it assumes that the Galactic parameters have been fixed during the last 4.6 Gyr. Although there are several studies that suggest that the spiral structure in the Galaxy is transient (Sellwood 2010, 2011), the evolutionary history of the Milky Way is quite uncertain, thus the Galactic model used is still valid. The study of the radial migration of the Sun under the influence of transient spiral arms implies to extend the space of Galactic parameters even more. Hence, simulations taking into account transient spiral structure will be carried out in a future work.

Recently, Minchev et al. (2013) made a more complex modelling of the Milky Way which involves self-consistent  $N$ -body simulations in a cosmological context together with a detailed chemical evolution model. They explored the evolution of a Galaxy for a time period of 11 Gyr, which is close to the age of the oldest disc stars in the Milky Way. They found that as the bar grows and the spiral structure start to form, the  $CR_{\text{bar}}$  and  $OLR_{\text{bar}}$  are shifted outwards of the disc producing changes in the angular momentum of stars. These changes in angular momentum can be doubled in the time interval from 4.4 to 11.2 Gyr. At the end of the simulation they found that stars of all ages end up at the solar neighbourhood ( $7 \leq r \leq 9$  kpc). Additionally, from the obtained metallicity distribution they conclude that the majority of stars come from inner regions of the Galactic disc ( $3 \leq r \leq 7$  kpc), although a sizeable fraction of stars originating from outside the solar neighbourhood is also observed. By assuming an error of  $\pm 1$  dex in the metallicity, they found that the possible region where the Sun was formed is between 4.4 and 7.7 kpc, with the highest probability to be around 5.6 and 7 kpc. These results support the conclusions of Wielen (1996).

According to Minchev et al. (2013), the Sun probably has migrated a distance between 1.5 and 2.9 kpc from the inner regions of the Galactic disc to  $R_\odot$ , which is different from what we obtained. The discrepancy in the conclusions is due to the fact that the structure of the Milky Way and its evolutionary history is quite uncertain. For instance, Minchev et al. (2013) argued that their results are strongly dependent on the migration efficiency in their simulations and also in the adopted chemical evolution model. We obtained a broad set of possible past Sun's orbits due to the large uncertainty in the bar and spiral arm parameters. Hence, a large-scale determination of the phase-space of stars together with better measurements of their chemical abundances are needed to constrain the history of the Milky Way and hence, their current properties. With the *Gaia* mission (Lindgren et al. 2008), we can expect to obtain the parallaxes and proper motions of one billion of stars very accurately. The *HERMES* (Freeman & Bland-Hawthorn 2002) and *APOGEE* (Allende Prieto et al. 2008) surveys, will provide a complete data base of chemical abundances and radial velocities for stars across all Galactic populations (bulge, disc and halo).

With a more accurate determination of the Galactic parameters (masses, scalelengths, pattern speeds), the motion of the Sun can be better constrained.

## 7 SUMMARY AND FINAL REMARKS

We studied the radial migration of the Sun within the Milky Way by computing its past orbit in an analytical potential representing the Galaxy. We took into account the uncertainties in the distance of the Sun from the centre of the Galaxy and its peculiar velocity components as well as the uncertainties in the bar and spiral arm parameters.

At the start of the simulations, the phase-space coordinates of the Sun are initialized to 5000 different positions and velocities which were obtained from a normal distribution centred at  $(r_\odot, v_\odot)$ , with standard deviations reflecting the uncertain present-day values of  $r_\odot$  and  $v_\odot$ . After performing the backward integration in time, we obtained a distribution of 'birth' phase-space coordinates. We computed the migration distribution function,  $p(R_p - R_b)$ , to study the amount of radial migration experienced by the Sun during the last 4.6 Gyr. We obtain the following results.

(i) For the majority of the simulations the median of the distribution  $p(R_p - R_b)$  is negative. This indicates that the motion of the Sun has been on average from outer regions of the Galactic disc to  $R_\odot$ .

(ii) The bar of the Milky Way does not produce considerable radial migration of the Sun. In contrast, the variation of amplitude and pattern speed of spiral arms produce migration on average of distances up to  $-1.8$  kpc, if the number of spiral arms is two. Hence, the birth radius of the Sun would then be around 11 kpc. In the case of a four-armed spiral potential, the Sun does not migrate on average; however, given that the width of the migration distribution  $p(R_p - R_b)$  can be up to 2.3 kpc, there is a probability of approximately 30 per cent that the Sun has migrated considerably from inner regions of the Galactic disc to  $R_\odot$ . If the potential of the Galaxy has multiple non-transient spiral patterns, the Sun does not migrate on average.

(iii) Only very specific configurations of the Galactic potential lead to considerable migration of the Sun. One case is when the separation of the  $OLR_{\text{bar}}$  and  $CR_{\text{sp}}$  is less than or equal to 1 kpc. Another case is when these two resonances overlap and are located further than 8.5 kpc from the Galactic Centre. For these cases there is a probability of up to 35 or 50 per cent that the Sun has experienced considerable radial migration from outer regions of the Galactic disc to  $R_\odot$ .

(iv) When the  $CR_{\text{sp}}$  is located between 7.3 and 8.4 kpc and the Galactic potential has four spiral arms, the probability that the Sun has migrated considerably from inner regions of the Galactic disc to its current position can be up to 30 per cent. For other combinations of bar and spiral arm parameters,  $P_{i-o} \sim 0$ . Hence, we found that in general it is unlikely that the Sun has migrated from inner regions of the Galaxy to  $R_\odot$ .

(v) Apart from the cases summarized above, we find that in general the Sun might not have experienced appreciable migration from its birth place to its current position in the Galaxy.

In this study, we consider the motion of the Sun in the plane. Simulations taking into account the vertical structure of the non-axisymmetric components of the Galactic potential will be carried out in future works (e.g Faure, Siebert & Famaey 2014; Monari et al. 2014 provide prescriptions for such potentials).

The study of the motion of the Sun during the last 4.6 Gyr has allowed us to determine its birth radius. This is the first step to understand the evolution and consequent disruption of the Sun's birth cluster in the Galaxy. In this respect, state of the art simulations are required to predict more accurately the current phase space of the solar siblings. In these simulations, internal processes such as self-gravity and stellar evolution have to be taken into account (Brown et al. 2010). A detailed study of the evolution and disruption of the Sun's birth cluster by using realistic simulations will appear in a forthcoming paper.

According to the above results, the current distribution on the  $xy$ -plane of the solar siblings will be different depending on the configuration of the Galactic potential. For the bar and spiral arm parameters that produce a broad migration distribution  $p(R_p - R_b)$  (cases where  $RSE \geq 1.7$  kpc), we expect a high dispersion of solar siblings, spanning a large range of radii and azimuths on the disc. For the Galactic parameters that do not generate a broad distribution  $p(R_p - R_b)$  (cases where  $RSE \leq 1$  kpc), we expect the Sun's siblings not to have a large radial dispersion. Therefore, depending on their final distribution, it would be likely or unlikely to find solar siblings in the near vicinity of the Sun.

Mishurov & Acharova (2011) concluded that it is unlikely to find solar siblings within 100 pc from the Sun, since members of an open cluster are scattered over a large part of the Galactic disc when the gravitational field associated with the spiral arms is taken into account. Consequently, a large-scale survey of phase space is needed. Only the *Gaia* mission (Lindegren et al. 2008) will provide data at the precision needed to probe for siblings which are far away from the Sun (Brown et al. 2010). The realistic simulations mentioned above will have to be exploited to develop methods to look for solar siblings among the billions of stars in the *Gaia* catalogue; however, together with the kinematics provided by the simulations, a complete determination of chemical abundances of stars has to be done to find the true solar siblings (Brown et al. 2010; Ramírez et al. 2014).

The identification of the siblings of the Sun will enable to put better constraints on the initial conditions of the Sun's birth cluster, instead of using only the current solar System properties (Adams 2010; Brown et al. 2010). With well-established initial conditions for the parental cluster of the Sun, the formation, evolution and current features of the Solar system could finally be disentangled.

## ACKNOWLEDGEMENTS

We want to thank Mercé Romero Gómez for providing us the model for the bar potential. Nathan de Vries and Inti Peluppesy for their valuable help that allowed us to make the interface of the Galactic model and to develop the `ROTATING BRIDGE`. We also want to thank the anonymous referee, Michiko Fujii, Lucie Jilková, Kate Tolfree and Teresa Antoja for their suggestions and fruitful discussions that improved this manuscript. This work was supported by the Nederlandse Onderzoekschool voor Astronomie (NOVA), the Netherlands Research Council NWO (grants #639.073.803 [VICI], #614.061.608 [AMUSE] and #612.071.305 [LGM]) and by the Gaia Research for European Astronomy Training (GREAT-ITN) network Grant agreement no.: 264895.

## REFERENCES

- Acharova I. A., Mishurov Y. N., Rasulova M. R., 2011, *MNRAS*, 415, L11  
 Adams F. C., 2010, *ARA&A*, 48, 47  
 Allen C., Santillán A., 1991, *Rev. Mex. Astron. Astrofis.*, 22, 255  
 Allende Prieto C. et al., 2008, *Astron. Nachr.*, 329, 1018  
 Antoja T., Figueras F., Romero-Gómez M., Pichardo B., Valenzuela O., Moreno E., 2011, *MNRAS*, 418, 1423  
 Athanassoula E., Romero-Gómez M., Masdemont J. J., 2009, *MNRAS*, 394, 67  
 Benjamin R. A. et al., 2005, *ApJ*, 630, L149  
 Bird J. C., Kazantzidis S., Weinberg D. H., 2012, *MNRAS*, 420, 913  
 Bissantz N., Gerhard O., 2002, *MNRAS*, 330, 591  
 Bonanno A., Schlattl H., Paternò L., 2002, *A&A*, 390, 1115  
 Bovy J. et al., 2012, *ApJ*, 759, 131  
 Brown A. G. A., Portegies Zwart S. F., Bean J., 2010, *MNRAS*, 407, 458  
 Casagrande L., Schönrich R., Asplund M., Cassisi S., Ramírez I., Meléndez J., Bensby T., Feltzing S., 2011, *A&A*, 530, A138  
 Churchwell E. et al., 2009, *PASP*, 121, 213  
 Comparetta J., Quillen A. C., 2012, preprint ([arXiv:1207.5753](https://arxiv.org/abs/1207.5753))  
 Contopoulos G., Grosbol P., 1986, *A&A*, 155, 11  
 Daflon S., Cunha K., 2004, *ApJ*, 617, 1115  
 Dehnen W., 2000, *AJ*, 119, 800  
 Dias W. S., Lépine J. R. D., 2005, *ApJ*, 629, 825  
 Drimmel R., 2000, *A&A*, 358, L13  
 Dwek E. et al., 1995, *ApJ*, 445, 716  
 Edvardsson B., Andersen J., Gustafsson B., Lambert D. L., Nissen P. E., Tomkin J., 1993, *A&A*, 275, 101  
 Faure C., Siebert A., Famaey B., 2014, *MNRAS*, 440, 2564  
 Feng F., Bailer-Jones C. A. L., 2013, *ApJ*, 768, 152  
 Ferrers N. M., 1877, *Pure Appl. Math.*, 14, 1  
 Freeman K., Bland-Hawthorn J., 2002, *ARA&A*, 40, 487  
 Freudenreich H. T., 1998, *ApJ*, 492, 495  
 Fuhrmann K., 2004, *Astron. Nachr.*, 325, 3  
 Fujii M., Iwasawa M., Funato Y., Makino J., 2007, *PASJ*, 59, 1095  
 Fujii M. S., Baba J., Saitoh T. R., Makino J., Kokubo E., Wada K., 2011, *ApJ*, 730, 109  
 Fux R., 2000, in Combes F., Mamon G. A., Charmandaris V., eds, *ASP Conf. Ser. Vol. 197, Dynamics of Galaxies: From the Early Universe to the Present*. Astron. Soc. Pac., San Francisco, p. 27  
 Gilmore G. et al., 2012, *The Messenger*, 147, 25  
 Gustafsson B., 1998, *Space Sci. Rev.*, 85, 419  
 Gustafsson B., 2008, *Phys. Scr. T*, 130, 014036  
 Gustafsson B., Meléndez J., Asplund M., Yong D., 2010, *Ap&SS*, 328, 185  
 Hammersley P. L., Garzón F., Mahoney T. J., López-Corredoira M., Torres M. A. P., 2000, *MNRAS*, 317, L45  
 Haywood M., 2008, *MNRAS*, 388, 1175  
 Holmberg J., Nordström B., Andersen J., 2009, *A&A*, 501, 941  
 Klačka J., Nagy R., Jurčí M., 2012, *MNRAS*, 427, 358  
 Lépine J. R. D., Roman-Lopes A., Abraham Z., Junqueira T. C., Mishurov Y. N., 2011a, *MNRAS*, 414, 1607  
 Lépine J. R. D. et al., 2011b, *MNRAS*, 417, 698  
 Lindegren L. et al., 2008, in Jin W. J., Platais I., Perryman M. A. C., eds, *Proc. IAU Symp. 248, A Giant Step: From Milli- to Micro- Arcsecond Astrometry*. Cambridge Univ. Press, Cambridge, p. 217  
 Lindegren L., Lammers U., Hobbs D., O'Mullane W., Bastian U., Hernández J., 2012, *A&A*, 538, A78  
 McLachlan R. I., 1995, *SIAM J. Sci. Comput.*, 16, 151  
 McLachlan R., Reinout G., Quispel W., 2002, *Acta Numer.*, 11, 341  
 Martínez-Valpuesta I., Gerhard O., 2011, *ApJ*, 734, L20  
 Martos M., Hernandez X., Yáñez M., Moreno E., Pichardo B., 2004, *MNRAS*, 350, L47  
 Matsumoto T., Hayakawa S., Koizumi H., Murakami H., Uyama K., Yamagami T., Thomas J. A., 1982, in Riegler G. R., Blandford R. D., eds, *AIP Conf. Proc. Vol. 83, The Galactic Center*. Am. Inst. Phys., New York, p. 48  
 Minchev I., Famaey B., 2010, *ApJ*, 722, 112  
 Minchev I., Quillen A. C., 2006, *MNRAS*, 368, 623  
 Minchev I., Boily C., Siebert A., Bienayme O., 2010, *MNRAS*, 407, 2122  
 Minchev I., Famaey B., Combes F., Di Matteo P., Mouhcine M., Wozniak H., 2011, *A&A*, 527, A147  
 Minchev I., Chiappini C., Martig M., 2013, *A&A*, 558, A9



Mishurov Y. N., 2006, *Astron. Astrophys. Trans.*, 25, 129  
 Mishurov Y. N., Acharova I. A., 2011, *MNRAS*, 412, 1771  
 Monari G., Helmi A., Antoja T., Steinmetz M., 2014, *A&A*, 569, 69  
 Nordström B. et al., 2004, *A&A*, 418, 989  
 Pelupessy F. I., van Elteren A., de Vries N., McMillan S. L. W., Drost N., Portegies Zwart S. F., 2013, *A&A*, 557, A84  
 Pichardo B., Martos M., Moreno E., 2004, *ApJ*, 609, 144  
 Pichardo B., Moreno E., Allen C., Bedin L. R., Bellini A., Pasquini L., 2012, *AJ*, 143, 73  
 Polyachenko E. V., 2013, *Astron. Lett.*, 39, 72  
 Portegies Zwart S. F., 2009, *ApJ*, 696, L13  
 Portegies Zwart S., McMillan S. L. W., van Elteren E., Pelupessy I., de Vries N., 2013, *Comput. Phys. Commun.*, 183, 456  
 Quillen A. C., Minchev I., 2005, *AJ*, 130, 576  
 Quillen A. C., Minchev I., Bland-Hawthorn J., Haywood M., 2009, *MNRAS*, 397, 1599  
 Quillen A. C., Dougherty J., Bagley M. B., Minchev I., Comparella J., 2011, *MNRAS*, 417, 762  
 Ramírez I. et al., 2014, *ApJ*, 787, 154  
 Recio-Blanco A. et al., 2014, *A&A*, 567, 5  
 Romero-Gómez M., Athanassoula E., Antoja T., Figueras F., 2011, *MNRAS*, 418, 1176  
 Roškar R., Debattista V. P., Quinn T. R., Stinson G. S., Wadsley J., 2008, *ApJ*, 684, L79  
 Schönrich R., Binney J., Dehnen W., 2010, *MNRAS*, 403, 1829  
 Sellwood J. A., 2010, *MNRAS*, 409, 145  
 Sellwood J. A., 2011, *MNRAS*, 410, 1637  
 Sellwood J. A., Binney J. J., 2002, *MNRAS*, 336, 785  
 Sofroniou M., Spaletta G., 2005, *Optim. Methods Softw.*, 20, 597  
 Valenti J. A., Fischer D. A., 2005, *ApJS*, 159, 141  
 Vallée J. P., 2002, *ApJ*, 566, 261  
 Weiland J. L. et al., 1994, *ApJ*, 425, L81  
 Weiner B. J., Sellwood J. A., 1999, *ApJ*, 524, 112  
 Wielen R., 1996, *A&A*, 314, 679  
 Zhao H., 1996, *MNRAS*, 278, 488

## APPENDIX A: A NEW APPROACH FOR PERFORMING REALISTIC SIMULATIONS:

### ROTATING BRIDGE

Spiral arms or bars rotate with some pattern speed, which means that the potential associated with these Galactic components will depend on time in an inertial frame. Hence, in order to compute the equations of motion of a set of stars in these Galactic components, it is convenient to choose a frame which corotates with the bar or with the spiral arms so that the potential of these perturbations will be time independent in the rotating frame.

Let us consider a star in a frame that corotates with the central bar or with the spiral arms. The Hamiltonian of this particle will be

$$H = \frac{\|\mathbf{p}\|^2}{2m} + U_T(\mathbf{r}) - (\Omega_p \times \mathbf{r}) \cdot \mathbf{p} - \frac{1}{2}m\|\Omega_p \times \mathbf{r}\|^2, \quad (\text{A1})$$

where  $\mathbf{r}$  and  $\mathbf{p}$  are the position and momentum vectors of the particle in the rotating frame,  $U_T(\mathbf{r}) = m(\phi_{\text{axi}}(\mathbf{r}) + \phi_p(\mathbf{r}))$  is the total potential energy due to the Galactic potential which is composed of an axisymmetric part  $\phi_{\text{axi}}(\mathbf{r})$  and a perturbation term  $\phi_p(\mathbf{r})$  that can be the bar or spiral arms (where  $m$  is the mass of the star). The last two terms of the Hamiltonian correspond to a generalized potential energy due to the rotating frame, where  $\Omega_p$  is the pattern speed of the bar or the spiral arms.

The above Hamiltonian can be written as

$$H = H_A + H_B, \quad (\text{A2})$$

where

$$H_A = \frac{\|\mathbf{p}\|^2}{2m}$$

$$H_B = U_T(\mathbf{r}) - m(\Omega_p \times \mathbf{r}) \cdot \dot{\mathbf{r}} - \frac{1}{2}m\|\Omega_p \times \mathbf{r}\|^2.$$

Note that  $\mathbf{p} = m\dot{\mathbf{r}}$ . A differential operator can be defined in terms of the Poisson bracket:

$$D_H = \{ \quad, H \} = \frac{\partial H}{\partial \mathbf{p}} \frac{\partial}{\partial \mathbf{r}} - \frac{\partial H}{\partial \mathbf{r}} \frac{\partial}{\partial \mathbf{p}},$$

so that the Hamilton's equations of motion can be written as

$$\dot{\mathbf{r}} = (D_{H_A} + D_{H_B}) \mathbf{r} \quad (\text{3a})$$

$$\dot{\mathbf{p}} = (D_{H_A} + D_{H_B}) \mathbf{p}. \quad (\text{3b})$$

By solving equations (A3a) and (A3b), we can express the time evolution of the position and momentum of a particle:

$$\mathbf{r}(t + \Delta t) = e^{(D_{H_A} + D_{H_B})\Delta t} \mathbf{r}(t) \quad (\text{4a})$$

$$\mathbf{p}(t + \Delta t) = e^{(D_{H_A} + D_{H_B})\Delta t} \mathbf{p}(t), \quad (\text{4b})$$

where  $e^{(D_{H_A} + D_{H_B})\Delta t}$  is the time evolution operator that is defined as

$$e^{(D_{H_A} + D_{H_B})\Delta t} = \prod_{i=1}^k e^{c_i H_A \Delta t} e^{d_i H_B \Delta t} + O(\Delta t^{n+1}), \quad (\text{A5})$$

where  $n$  is an integer which corresponds to the order of the integrator.  $(c_i, d_i)$  ( $i = 1, 2, \dots, k$ ) is a set of real numbers. The simplest case is when the integrator has second order. This integrator, called Leapfrog, has the following coefficients:  $n = 2$ ,  $c_1 = 0$ ,  $d_1 = \frac{1}{2}$ ,  $c_2 = 1$ ,  $d_2 = \frac{1}{2}$ . Those are the coefficients used in the interface of BRIDGE for AMUSE. In Section A1, we will mention briefly the coefficients used in AMUSE for high-order integrators. The operators in equation (A5) are applied to  $r$  and  $p$  in the order  $(c_1, d_1, \dots, c_k, d_k)$ .

The kick (K) operator or  $e^{H_B \Delta t}$  produces the following set of equations:

$$\dot{\mathbf{r}} = 0 \quad (\text{6a})$$

$$\dot{\mathbf{p}} = \mathbf{F}, \quad (\text{6b})$$

where  $\mathbf{F}$  is the total force of the particle in the rotating frame, which is given by

$$\mathbf{F} = m\mathbf{a} - m\Omega_p \times (\Omega_p \times \mathbf{r}) - 2m(\Omega_p \times \mathbf{r}). \quad (\text{A7})$$

Here  $\mathbf{a} = -\nabla(\phi_{\text{axi}}(\mathbf{r}) + \phi_p(\mathbf{r}))$ . In case of having a central bar and spiral arms, one rotating frame has to be chosen first to make the integration of the equations of motion. We chose a frame that corotates with the bar. Every time step  $\Delta t$ , the force of the axisymmetric component plus bar is computed; since spiral arms have a different pattern speed, the position of the star is calculated in another frame that corotates with the spirals; there, the force due to this perturbation is computed. Finally, the position goes back to the corotating frame with the bar to calculate the total force.

Given that the momentum can also be written as  $\mathbf{p} = m\mathbf{v}$ , equations (A6a) and (A6b) can be written as

$$\dot{x} = \dot{y} = \dot{z} = 0 \quad (\text{8a})$$

$$\dot{v}_x = a_x + \Omega_p^2 x + 2\Omega_p v_y \quad (\text{8b})$$

$$\dot{v}_y = a_y + \Omega_p^2 y - 2\Omega v_x \quad (8c)$$

$$\dot{v}_z = a_z. \quad (8d)$$

The solution to this system of equations is

$$v_x(t + \Delta t) = \left[ v_x(t) - \left( \frac{a_y + \Omega^2 y}{2\Omega} \right) \right] \cos(2\Omega\Delta t) + \left[ v_y(t) + \left( \frac{a_x + \Omega^2 x}{2\Omega} \right) \right] \sin(2\Omega\Delta t) + \frac{a_y + \Omega^2 y}{2\Omega} \quad (9a)$$

$$v_y(t + \Delta t) = \left[ v_y(t) - \left( \frac{a_x + \Omega^2 x}{2\Omega} \right) \right] \sin(2\Omega\Delta t) + \left[ v_x(t) + \left( \frac{a_y + \Omega^2 y}{2\Omega} \right) \right] \cos(2\Omega\Delta t) - \frac{a_x + \Omega^2 x}{2\Omega} \quad (9b)$$

$$v_z(t + \Delta t) = v_z(t) + a_z \Delta t. \quad (9c)$$

On the other hand, the drift (D) operator or  $e^{H_A \Delta t}$ , produces this set of equations:

$$\dot{x} = p_x \quad (10a)$$

$$\dot{y} = p_y \quad (10b)$$

$$\dot{z} = p_z \quad (10c)$$

$$\dot{p}_x = \dot{p}_y = \dot{p}_z = 0, \quad (10d)$$

which give the solution:

$$x(t + \Delta t) = x(t) + v_x(t + \Delta t) \Delta t \quad (11a)$$

$$y(t + \Delta t) = y(t) + v_y(t + \Delta t) \Delta t \quad (11b)$$

$$z(t + \Delta t) = z(t) + v_z(t + \Delta t) \Delta t. \quad (11c)$$

In the more general case of having a star cluster with self-gravitating particles, its Hamiltonian will be

$$H = \sum_i^n \frac{\|\mathbf{p}_i\|^2}{2m_i} - \sum_{i<j}^n \frac{Gm_i m_j}{\|\mathbf{r}_{ij}\|} + \sum_i m_i (\phi_{\text{axi}}(\mathbf{r}_i) + \phi_p(\mathbf{r}_i)) - \sum_i (\Omega_p \times \mathbf{r}_i) \cdot \mathbf{p}_i - \frac{1}{2} \sum_i m_i \|\Omega_p \times \mathbf{r}_i\|^2, \quad (A12)$$

which can be separated as equation (A1) with the terms

$$H_A = \sum_i^n \frac{\|\mathbf{p}_i\|^2}{2m_i} - \sum_{i<j}^n \frac{Gm_i m_j}{\|\mathbf{r}_{ij}\|}$$

$$H_B = \sum_i m_i (\phi_{\text{axi}}(\mathbf{r}_i) + \phi_p(\mathbf{r}_i)) - \sum_i (\Omega_p \times \mathbf{r}_i) \cdot \mathbf{p}_i - \frac{1}{2} \sum_i m_i \|\Omega_p \times \mathbf{r}_i\|^2.$$

For this system, the kick operator gives the same set of velocities as in equations (A9a)–(A9c); nevertheless, when the drift operator is applied, additionally to the position, the velocity of the particles has to be updated again by taking into account their gravitational interaction, as is explained in section 2 of Fujii et al. (2007).

## A1 High-order integrators

In AMUSE several high-order integrators have been implemented from 4th until 10th order. In the case of fourth-order integrators, they can have 4, 5 or 6 stages (named M4, M5 or M6); that is, the number of times the force is computed when is applied equation (A5). The coefficients used in those integrators are the ones found by McLachlan (1995) and McLachlan, Reinout & Quispel (2002). The sixth-order integrators implemented in AMUSE are of 11 and 13 stages (M11 and M13), with the coefficients found by Sofroniou & Spaletta (2005). In the simulations performed here, we used the ROTATING BRIDGE with a sixth-order integrator.

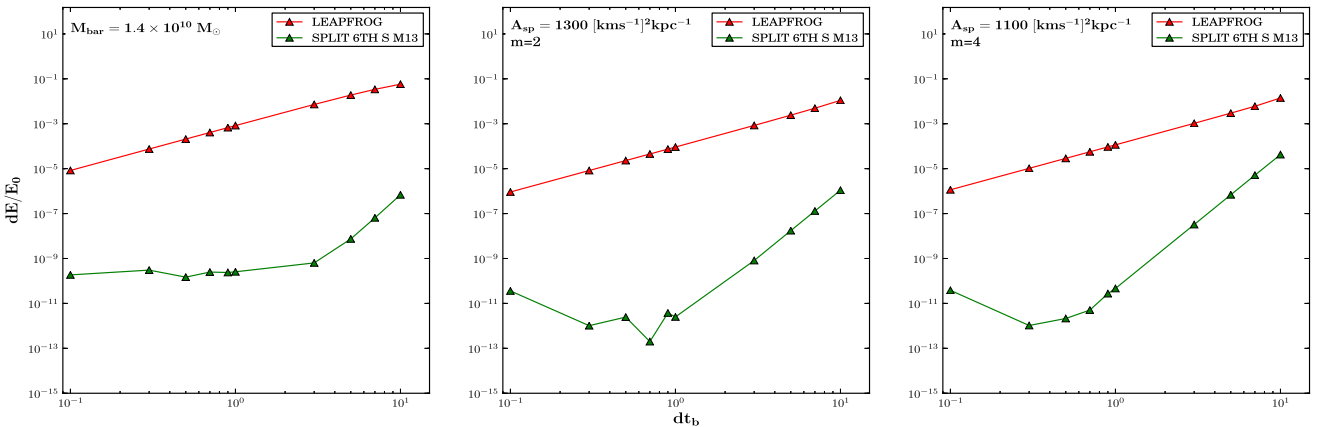


**Figure A1.** Fractional energy error as a function of the ROTATING BRIDGE time step when the Galactic potential is composed by – left: axisymmetric part + central bar. Middle: axisymmetric part + two spiral arms. Right: axisymmetric part + four spiral arms. The fractional energy error was computed by using a star with the following galactocentric initial position and velocity:  $\mathbf{r} = (-8.5, 0, 0)$  kpc;  $\mathbf{v} = (11.1, 12.24 + V_{\text{LSR}}, 0)$  km s $^{-1}$ .  $V_{\text{LSR}}$  is the velocity of the local standard of rest.

In order to assess the accuracy of the code, we computed the energy error as a function of the `ROTATING BRIDGE` time step ( $dt_b$ ) for a solar orbit under different bar and spiral arm parameters. The results are shown in Fig. A1. Note that for a fixed  $dt_b$  the sixth-order Leapfrog can be six orders of magnitude more accurate than the second order Leapfrog. We found that such accuracy is independent from the bar and spiral arm parameters, as also can be seen from Fig. A1.

We chose a  $dt_b$  of 0.5 Myr for the simulations, which corresponds to an energy error of the order of  $10^{-10}$  when the Galactic potential has only a central bar or spiral arms.

This paper has been typeset from a  $\text{\TeX}/\text{\LaTeX}$  file prepared by the author.